HIGH-POWER DIODE LASER SURFACE HARDENING WITHIN A MACHINING CENTER

HIGH-POWER DIODE LASER SURFACE HARDENING WITHIN A MACHINING CENTER

By

JEREMIAH J. STENEKES, B.ENG.

A Thesis

Submitted to the Faculty of Graduate Studies

in Partial Fulfillment of the Requirements

for the Degree of

Master of Applied Science

McMaster University

Master of Applied Science
Mechanical Engineering

McMaster University
Hamilton, Ontario

TITLE:	High-Power Diode Laser Surface Hardening within a Machining Center
AUTHOR:	JEREMIAH J. STENEKES, B.ENG.
SUPERVISORS:	Dr. Philip Koshy Dr. Mohamed A. Elbestawi
NUMBER OF PAGES:	xiii, 109

Abstract

Flexible manufacturing systems and lean production philosophies are in increasing industrial demand. Multiple manufacturing processes integrated into stand alone automated equipment can be utilized to greatly reduce operation costs. New technologies are continually being developed that can be easily combined with related manufacturing processes. Flexible machining and surface hardening operations can be realized in a single set-up by integrating a high-power diode laser (HPDL) within a machine tool structure.

The following research presents the concept of integrated laser surface hardening within a machine tool environment. Experimental work was performed using a HPDL for transformation hardening of AISI 4140 steel.

Both quasi-steady analytical and transient finite element heat transfer models have been developed. Solutions of the models are compared, which show that the more sophisticated finite element modeling is necessary only if accuracy of peak surface temperature is important. Otherwise, the simpler but faster analytical model can be used to describe the temperature profiles during laser heating.

A novel approach using themperature indicating lacquers was shown to be a simple and reliable tool for temperature measurement. The analytical model was further used to find a best fit with the experimental measurements to estimate the

fraction of laser power absorbed by the workpiece surface. With the aid of the model, it was shown that the austenite transformation temperature is highly dependent on the scanning speed. For slower speeds, the transform temperature was closer to the A_3 temperature given by the iron-iron carbide phase diagram. Tests performed at faster scanning speeds indicated transformation temperatures as high as 1230 °C.

Experiments were divided into three series. The first series was performed at slow scanning speeds (200-1000 mm/min) and low laser powers (200-500 W). Hardening was executed on flat workpieces with the laser scanning along a linear path. The second and third test series were performed at fast scanning speeds (2000-8000 mm/min) and higher laser powers (1000-2000 W) with hardening done on rotating cylindrical workpieces. The third tests series consisted of two laser passes in an attempt to increase the penetration depth of the hardened layer. These tests resulted in severe distortion due to melting that would require nearly the entire hardened layer to be machined away post heat treatment. However, if the melting temperature is not significantly exceeded multiple laser passes could be used to increase the thickness of the hardened layer.

Higher case depths were realized for the slow tests since these tests have a greater laser-work interaction time. During laser treatment, the uncoated workpieces were left exposed to allow for oxidation and melting in order to increase the fraction of absorbed laser power. The absorptivity is shown to be a high as 85% for these

tests.

Results are presented in a form useful in selection of laser power and scanning speed to obtain the desired level of hardening, without having to resort to complex analytical or numerical models. Investigations into in-process monitoring show that measurement of surface temperature using an infrared thermometer could be used to control the generated hardened layer reducing process scrap.

Acknowledgements

I would like to share my appreciation for my supervisor Dr. Philip Koshy for his dedicated support and valuable direction. I am grateful for his encouragement and for the taking great quantities of his time to help me with my work. Additionally, I would like to thank Dr. Eugene Ng for the time spent discussing the various issues and challenges I faced during my research.

I am grateful for the opportunity to study at McMaster University within the McMaster Manufacturing Research Institute. I am indebted toward Dr. Mohamed Elbestawi for providing me with this opportunity.

Special thanks to Mr. Warren Reynolds and Mr. Jim McLaren for countless hours of assistance given to me when preparing for and performing my experiments. I also, would like to thank Mr. Joe Verhaeghe, Mr. Doug Culley, Mr. Chris Butcher, Mr. Dave Schick, Mr. Mark MacKenzie and Mr. Ron Lodewyks for countless help with my experimental work.

Finally, I would like to thank my wonderful fiancée Ms. Jennifer Boyd for her informed opinions, our endless discussions and most of all for the much needed encouragement she gave me.

Contents

List of Tables

List of Figures

CHAPTER 1
Introduction

Currently there is focused effort in the manufacturing sector towards increasing equipment process flexibility and decreasing material and operation waste. Existing and emerging technologies alike are being streamlined to minimize manufacturing setup time and eliminate non-value adding processes.

Surface hardening processes have been overlooked in the effort to address these trends. This is a critical oversight as surface treatments, in many cases, form the bottleneck of a production system. Heat treatment processes that require little set-up time such as carburizing often require long production cycle times. The opposite is observed in induction hardening. Minimizing both set-up and production times is key with respect to lowering manufacturing costs. To this end employing new surface hardening techniques could allow for substantial gains in process efficiency and clearly warrant further investigation. Integration of a high power diode laser (HPDL) into a machine tool suggested by Hügel et al. [1] is a novel approach to achieving these goals, allowing for high flexibility and leaner production. Furthermore, by integrating surface hardening with other manufacturing operations transfer time between manufacturing cells can be virtually eliminated.

1.1 Surface Transformation Hardening

Surface hardening is used to improve the wear resistance of a material without affecting the softer and tougher inner bulk of the workpiece. An advantage of surface over through hardening is that surface hardening can be used to treat less expensive low and medium-carbon steels without major distortion and cracking.

Classification of surface hardening processes can be divided into two groups. The first involves adding material to the surface and the second employs surface modification without the addition of material. Materials can be added to the workpiece surface through thin films, coatings, claddings and by altering the chemical composition at the surface through diffusion. Alteration of steels by diffusion is usually performed by heating the workpiece in a furnace in an atmosphere rich with the solute species that is to be added. The additional material can be used to increase the hardening potential of a low-carbon steel which otherwise may not contain sufficient carbon for surface hardening by a strictly thermal process. The effectiveness of diffusion methods are limited by long process times and inefficient use of energy. Diffusion processes require heating of the entire workpiece including surfaces that do no demand hardening. Common diffusion methods include, carburizing, nitriding, carbonitriding, nitrocarburizing and boriding, where carbon, nitrogen and/or boron are added to the material surface.

Surface hardening of steel without the addition of material does not require

treatment of the whole component, requiring less input energy. The nature of the process can be either thermal or mechanical. Inexpensive mechanical processes such as shot peening are used to work harden the material surface and induce compressive residual stresses on the component surface. This results in a non-uniform shallow hardened layer.

Thermal or transformation processes are the most common and work the same way as through hardening. Steel that is thermally hardened is heated beyond the transition temperature given by its phase diagram such that a transformation occurs in the material microstructure. At room temperature only 0.006% carbon is soluble in iron which exists in a body centered cubic (BCC) arrangement called ferrite. Carbon, which is harder than iron, exists in the materials microstructure as iron carbide (Fe_3C) called cementite. When heated above a certain temperature iron transforms to a face centered cubic (FCC) arrangement (austenite) and carbon is much more soluble. Carbon then diffuses into the FCC structure until a homogeneous composition is formed. Upon cooling the carbon diffuses back out of the austenite phase so that ferrite and cementite phases are reformed. If the material is cooled quickly (quenched) then there may not be sufficient time for the dissolved carbon to diffuse out of the iron. In this case grains of a hard phase called martensite remains. For treatments where the heated surface layer comprises a large fraction of the workpiece, quenching is performed using a liquid (often water or oil) to quickly transfer heat out of the

workpiece by convection. If the heated layer is a small fraction of the workpiece volume the surface may be self-quenched, where the heat is quickly conducted away from the surface into the cooler inner bulk material.

Process methods for surface transformation hardening are induction hardening, arc hardening, flame hardening, electron beam hardening and laser surface hardening. In laser hardening, radiation energy is absorbed at a localized region of the workpiece surface, transforming its microstructure. A comparison of laser hardening with a variety of surface hardening processes is outlined in Table 1.1. Laser hardening has many advantages over other surface treatments such as:

- It can be used selectively. The laser can be scanned only over the areas that require hardening. Diffusion methods uncontrollably treat every exposed workpiece surface, wasting energy.

- Laser hardening is a flexible process. When the laser is attached to a CNC machine tool or robot, new processes can be reprogrammed without adding or

Table 1.1: Comparison of surface hardening methods [2].

Parameter	*Laser*	Induction Hardening	Carburizing	Flame	Arc	Electron Beam
Max. Treatment Depth, mm	*1.5*	5	3	10	10	1
Distortion	*Very* low	Medium	Medium	High	Medium	Very low
Flexibility	*High*	Low	Medium	High	High	Medium
Precision	*High*	Medium	Medium	Low	Low	High
Operator skill	*Medium*	Medium	Medium	High	High	Medium
Environmental Impact	*Low*	Low	High	Medium	Medium	Low
Quenchant required	*No*	Sometimes	No	Yes	No	No

redesigning equipment. Induction hardening requires a coil to be designed for every component. Design and manufacture of new coils cost time and resources.

- Hardening with a laser is very repeatable. The temperature field generated by flame and arc heating are very difficult to control and lead to very imprecise hardened layers.

- Negative environmental impacts due to quenching are eliminated in laser hardening as no petroleum products are required as quenching media. Quenchants used in other processes may evaporate upon heating and cause environmental and safety problems at the workplace.

- Heat treating with a laser can be performed in atmospheric conditions. Electron beam hardening requires the process to be performed in a vacuum. Production rates for electron beam hardening are typically low due to vacuum pumping, and part size is limited by the chamber.

Even with the many advantages of laser surface hardening, the technology has not been widely utilized in industry. Until recently, only CO_2 lasers have possessed the necessary power density and spot size required for practical hardening applcations. Due to the high reflectivity of the laser beam on metallic surfaces a coating is generally required to achieve realistic laser absorptivity. Recently high-power neodymium-doped yttrium aluminium garnet (Nd-YAG) lasers have also been shown

to be effective for laser hardening as the surface absorptivity is higher. However, the cost of these laser systems is high, making laser hardening uneconomical for most applications.

1.2 High-Power Diode Laser (HPDL) Materials Processing

More recently diode lasers have been improved and output powers high enough for hardening applications have been realized. Currently, 10 kW HPDL with 0.6 x 3.0 mm^2 spot size are commercially available with more powerful lasers becoming available every few years. HPDL are available at much lower costs than CO_2 and Nd-YAG lasers and are more efficient. Their compact size makes them ideal for integration into manufacturing systems, such as machine tools. High wall to beam efficiency, low laser-work reflectivity, low maintenance and the ability to transport the beam with fiber optics makes HPDL ideal for many industrial applications including surface hardening.

Although power densities are still lower for HPDL than CO_2 and Nd-YAG systems, many applications can benefit from HPDL. Power densities up to 10^3 W/mm^2 for HPDLs [4] are typical. Figure 1.1 shows the required power densities against laser-work interaction time for a number of applications. Typical HPDL applications include soldering of electronic components, brazing, surface hardening, cladding and laser assisted machining [4]. However, applications such as deep welding and cutting require a high laser beam power density not currently available with HPDL systems.

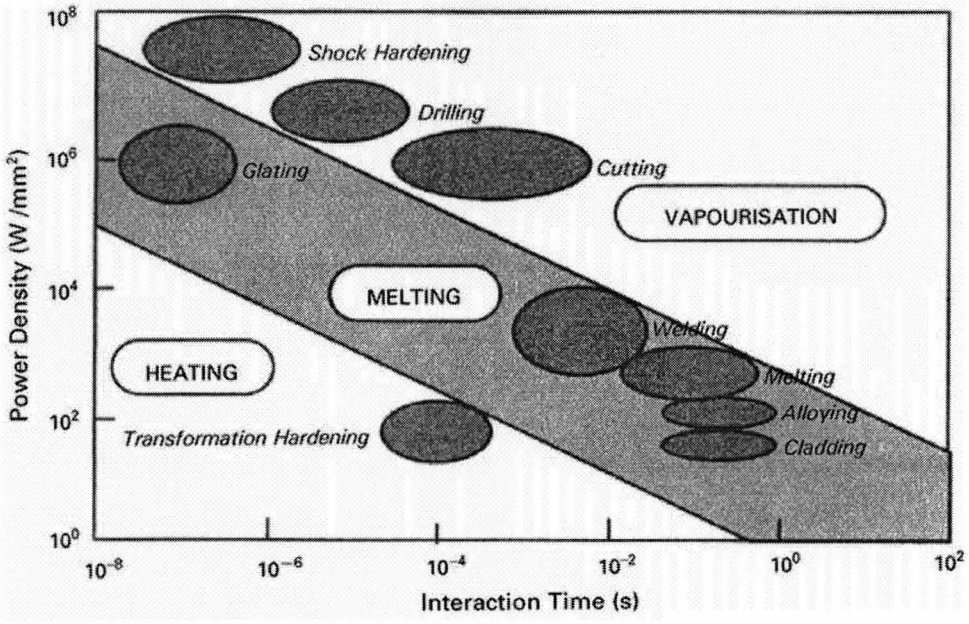

Figure 1.1: Laser materials processing application requirements on power density and interaction time [3].

1.3 Laser Integrated Flexible Manufacturing

Dedicated manufacturing systems are increasingly becoming replaced by flexible computer controlled systems. The advantage of flexible systems is that new production work can be quickly implemented with minimal design and fabrication of manufacturing systems. Machining lead times have been greatly reduced owing to the use of CNC machine tools. Integration of multiple manufacturing operations into a single set-up has reduced costs by eliminating non-value adding transfer steps. This has been shown to improve part quality as the number of fixturings per component is minimized. Industries such as aerospace and medical have benefited by reducing start-up time and performing multiple tasks with the same equipment, while the automotive industry has benefited by eliminating non-value adding processes.

A typical manufacturing process for a cam or crank shaft would first require a rough machining stage. The work in process would then be transferred off the machine tool and sent to a furnace for a diffusion controlled surface hardening process. Heat treatment requires hours as the hardened depth is determined by the time allowed for diffusion. Once heat treatment is finished the work is sent back to a machine tool where it must be reloaded for finishing machining.

By integrating laser surface hardening within a machine tool, production time and cost can be reduced considerably. This allows machining and hardening operations to be performed in one set-up. In addition, the flexibility of the laser eliminates the need to make design changes to the manufacturing equipment for new components. Only a new computer controlled tool path and process parameters (i.e. laser power, focal distance and scanning speed) are required.

Previous researchers have taken considerable care to avoid oxidization of the steel workpiece by processing the material in an inert atmosphere as the resultant oxide layer is found undesirable for most applications. Surface melting is also avoided in order to maintain surface quality. Avoiding oxidation and melting is not necessary with laser hardening when performed in a machine tool as a finish machining stage post heat treatment can easily remove these unwanted effects. Indeed, by purposely allowing oxidization and melting, the surface absorptivity may be enhanced, improving the overall efficiency of the process and increasing the maximum attain-

able hardened depth. Machining a hardened part may also improve the final surface finish. As shown in Figure 1.2, better surface finish correlates to machining material above a threshold hardness. The surface finish prior to hardening may affect the absorptivity as well; the ability to choose rough machining parameters to generate a specific surface topography may also enhance laser absorptivity.

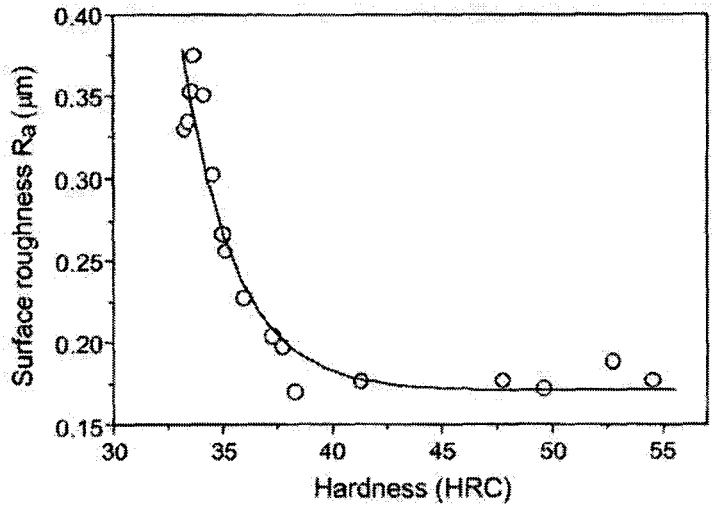

Figure 1.2: Machined surface roughness as a function of work hardness [5].

1.4 Scope and Organization of Present Work

It is the aim of the present work to prove the concept of laser surface hardening within a machine tool. Problems associated with laser hardening such as process selection, rapid thermal cycles, temperature and absorptivity measurement and in-process monitoring are addressed.

The work material used is AISI 4140 steel which has good hardenability and a wide range of applications such as cam shafts, gears, sprockets, tool holders and

hydraulic machinery shafts. Many applications of this steel require surface hardening and precision machining making it an ideal material for integrated laser hardening within a machine tool.

A large fraction of previous research performed in laser surface hardening deals with the development of heat transfer models to aid in process parameter selection. As most of this research is for CO_2 lasers in ideal conditions the absorptivity can be considered uniform over a limited range of process parameters. In this work, a HPDL is used as the processing laser which has greater laser-work absorptivity for metallic surfaces, although the absorptivity can change considerably with varying process conditions. This work investigates changes in absorptivity, and with the aid of a simple heat flow model presents strategies that could be used to choose process parameters easily with no need for complicated models.

Many experiments indicate uneven surfaces after heat treatment due to melting. Required finish machining depths were assessed for removal of the deformed surface. The finish depth of cut was defined by the minimum amount of material removal required for a uniform finished surface. Process selection strategies developed were then geared to account for finish machining.

In-process monitoring with the use of an infrared thermometer was also investigated. Relationships are shown that could be used to correlate emissive infrared radiation measurements from the surface to the final hardened depth. With the ad-

dition of a closed loop control system, process parameters could be altered in-process to improve final part quality and minimize scrap.

CHAPTER 2
Literature Review

Laser transformation hardening is a thermal process whereby heat from a laser is used to transform a material's microstructure. Unlike traditional transformation hardening processes, the heating cycle is very rapid. For non-rapid heating cycles the time dependency of the formation of austenite can be neglected. However, for laser hardening it cannot, and rapid heat treatment effects must be considered. A review of rapid heat treatment and the formation of austenite are offered in this chapter.

In the past, laser hardening has been performed using large and expensive CO_2 or Nd-YAG laser systems. In this work, a more practical HPDL is used which has many advantages for laser hardening when compared to competing technologies. A description of HPDL technology and its associated advantages is covered in this following text. Additionally, a survey of laser hardening studies using an HPDL is presented.

Process explanation and optimization can be achieved through experimentation or modeling. As laser hardening is a transient process and many changes cannot be easily measured through experiment, the majority of past research has put emphasis on heat flow and phase transformation modeling. A review of the development of analytical and numerical models can be found in the later sections of this chapter.

2.1 Rapid Heat Treatment

Conventional furnace based heat treatment is a slow process where steel is hardened by raising its temperature above the transformation temperature indicated by the steel's phase diagram. At this point the steel can be assumed to be fully austenitized and is said to have phase equilibrium. Hardness is then determined from the quenching rate given by the continuous cooling transformation (CCT) diagram. Rapid heat treatment is a process where the steel is quickly heated above its transformation temperature. The assumption that full austenitization occurs above transformation temperatures given by the phase diagram no longer holds. The reality of the process is that austenite formation is dependent on time. This time dependency varies directly with the speed of the heating cycle. In order to austenitize material with rapid heating cycle the maximum temperature must be elevated above the transformation temperature indicated by the corresponding steel phase diagram. The maximum temperature required is proportional to the rate of the heating cycle.

The dissolution of austenite which has been studied in greater detail than its formation can be limitedly determined by the CCT diagram. Cooling by self-quenching is typically very rapid and most of the austenitized steel can be assumed transformed to martensite. Under such rapid cooling conditions, some of the austenite may be retained, especially when carbon content is high. Use of the CCT diagram is limited because it assumes full austenitization prior to cooling.

2.1.1 An Overview of Rapid Heat Treatment

Although the formation of austenite has not been as extensively investigated as its decomposition, a number of inquiries have been made. The first report on the mechanism of austenite formation by heating was made by Arnold and McWilliams [6] who stated that austenite formation is a process of nucleation and growth. The rate of nucleation and growth has been studied in ferrite-cementite aggregates [7–10] and in pearlite colonies [11, 12]. Roberts and Mehl [7] experimentally investigated austenite formation in ferrite-cementite aggregates reporting that the rate of nucleation and rate of growth are structure sensitive properties and increase with increasing temperature above the phase diagram transition temperature.

The formation of an austenite nucleus begins at a ferrite/cementite interface, the specific locations at which nuclei are formed being a matter of probability. Figure 2.1 shows austenite nucleation sites in steels for ferritic, spheroidized and pearlitic microstructures. In pearlite, it has been reported that nucleation of austenite occurs primarily at both pearlite colony intersections [10] and throughout the pearlite matrix at ferrite/cementite interfaces [7]. In spheroidized steels, nucleation occurs at a carbide particle and grows along the boundary; further growth occurs into the ferrite matrix and is controlled by diffusion [10], although when carbon dispersion is fine, nuclei do not appear at every carbide particle as some are consumed by growing austenite grains. Kaluba et al. [13] realized a bainite like austenite morphology during

the early stages of austenitization when rapidly heating 0.68% C steel of an annealed ferrite with coarse spheroidized cementite microstructure. This meant that at the early stages of austenite formation carbon can exist as finely distributed cementite regions before homogenization.

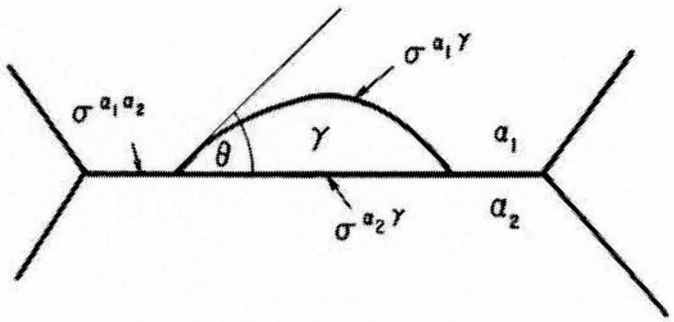

Fig. 9—Austenite nucleation at ferrite grain boundary.

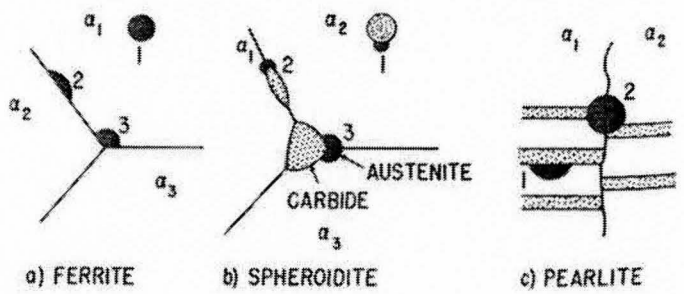

Figure 2.1: Nucleation sites for Austenite in steel [10].

Growth of austenite nuclei is a diffusion controlled process influenced by the concentration and temperature gradients through the material. The rate of reaction between cementite and ferrite into austenite is dependent on the rate of solution at the interface and on the rate of migration of carbon in austenite [7]. Independent of temperature, the degree of the carbon concentration gradient is limited by the distance between carbide particles. An increase of interlamellar spacing in pearlite or

an increase in the coarseness of carbon dispersion in spheroidized steels will result in a decrease of the concentration gradient. Figure 2.2 shows three diffusion situations for the dissolution of pearlite based on the carbon content. The first situation for hypoeutectoid alloys results in a mixture of austenite and ferrite, the second situation for eutectoid alloys produces austenite alone and the third for hypereutectoid alloys will yield austenite and cementite. Further heating will fully dissolve any remaining non-austenite phases and the material will become fully austenitized.

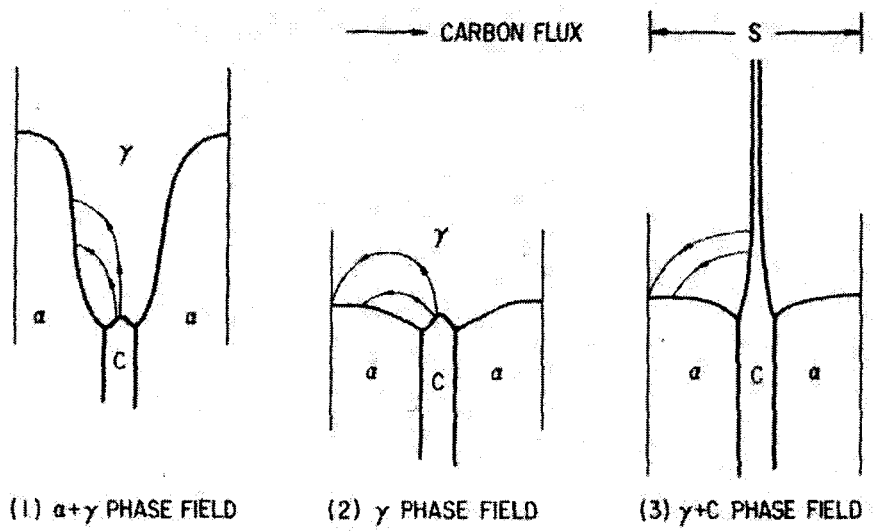

Figure 2.2: Diffusion geometries for the dissolution of pearlite [10].

Efforts have been made to analytically model austenite formation from ferrite-carbide aggregates [9–11]. Analytical models assume that diffusion of carbon through austenite is the rate limiting step, where the growth of austenite depends on the movement of both the cementite/austenite and austenite/ferrite boundaries. Molinder [14] however found that for a high carbon steel 1.27% C, carbon diffusion is not

the rate limiting factor of cementite dissolution, but instead the rate of disintegration of cementite at the interface determines this rate. Judd and Paxton's [9] model found excellent correlation between calculated and experimental data for zone-refined Fe-C alloy, but did not for Fe-0.5% Mn-C alloy and a low carbon steel. Speich et al. [10] presented two analytical models of pearlite dissolution into austenite. The first model simplified the solution for the concentration field and due to unrealistic assumptions [12] does not find good agreement with experimental results. The second model indicated the pearlite dissolution rate as a function of temperature and interlamellar spacing and yielded better results when compared with measured growth rates as shown in Figure 2.3. Hillert et al. [11] recognized that when the distance between cementite particles is large the cementite is quickly consumed by austenitized steel where subsequent formation of austenite is controlled by carbon diffusion.

Numerical models [12, 15–18] have also been developed for ferrite/cementite microstructures and dissolution of pearlite. Akbay et al. [17] developed one-dimensional finite difference models for idealized planar and spherical Fe-C microstructures which were compared with exact solutions. Jacot et al. [12] proposed a two-dimensional model for the reaustenitization from pearlite to predict dissolution rate, interface shape and concentration field in austenite as a function of temperature for various lamellae spacing. The term reaustenitization is used since austenite formation is a structure sensitive process determined by original austenite decomposition upon

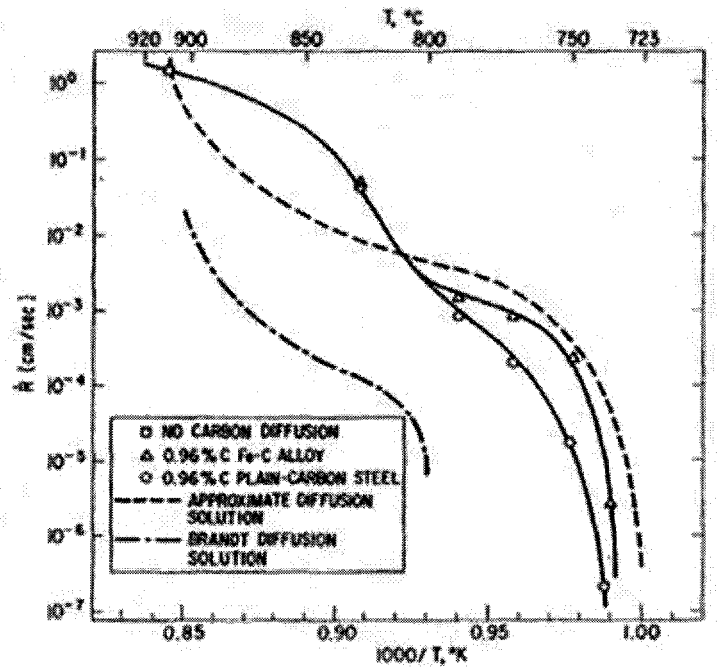

Figure 2.3: Predicted and measured growth rates of austenite from pearlite [10].

cooling. The model assumed local equilibrium at phase interfaces. It was shown that steady-state growth breaks down at temperatures much greater than the initial transformation temperature.

2.2 Laser Transformation Hardening

Laser hardening is a rapid heat treatment process whereby a material surface is locally heated by focused laser radiation. Heat is absorbed by the atoms at the surface of the material and transferred further into the material by conduction. If sufficient heat is stored by the workpiece, material austenitization will occur. Quenching is self-induced by the cool bulk mass of the workpiece, allowing any austenitic steel to be transformed into martensite. The resulting workpiece has a hardened surface with

increased wear and fatigue resistance while toughness is left uncompromised within the workpiece core.

Application of lasers for material heat treatment has been reported as early as the 1960's [2], but had not been researched seriously as a practical industrial process until the late 1970s [19, 20]. The first report of laser hardening used in large scale industrial production seems to be by General Motors in 1973 [21, 22] where internal selective laser hardening of a ferritic malleable iron power steering housing bore was performed to increase the service life of the component [23]. The resulting housing had five tracks of hardness 58-62 HRc that were 1.5-2.5 mm wide and 0.25 mm deep. Decreased wear rates to just 10% of unhardened housings were found. Laser hardening was advantageous in that the laser beam could be easily aimed within the internal surface of the housing bore. Alternative solutions to laser treatment required changing to a tougher component material which would present difficulties with machining.

2.2.1 Laser Technology

Traditionally laser hardening had been achieved with CO_2 or Nd-YAG lasers, as these were the only practical technologies capable of producing continuous wave beams at the required power levels. Unfortunately these lasers are expensive as a result of low operating efficiencies, large size of the laser head, and high investment cost. While CO_2 lasers have large output powers they produce a beam with a large wavelength of 10,600 nm that is mostly reflected by metal surfaces. Laser hardening

using a CO_2 laser requires that an absorbent coating be applied to a workpiece surface. Nd-YAG lasers have an improved beam wavelength size of 1,060 nm that is better absorbed by metals, but are very expensive in both operating and investment cost. The Gaussian beam profile of these lasers is not very desirable for hardening and requires expensive focusing optics to produce a uniformly hardened profile across the laser track width. The cost and difficultly of utilizing these lasers has significantly curtailed interest in laser surface hardening.

Recently, diode lasers have been developed that compete well with other high power lasers for industrial processes. Since the early 1990s where a diode laser of 15 W was reported performing a soldering application, diode lasers have evolved and can now produce up to 10 kW. Diode lasers able to produce more than 0.5 W have been termed high powered diode lasers (HPDL) [3]. Diode lasers are also more efficient, have a lower investment cost and produce a laser beam with lower wavelengths (790-980 nm) that is more easily absorbed by metal surfaces. The beam profile for HPDL is also ideal for hardening as it is top hat along the spot length. Table 2.1 summarizes a comparison of HPDL, CO_2 and Nd-YAG lasers. The small laser light wavelength greatly improves metal absorption when compared with CO_2 lasers and is slightly better than Nd-YAG. The energy not absorbed at the material surface is reflected, the reflectivity as a function of wavelength is shown in Figure 2.4 for a variety of metals.

Table 2.1: Comparison of Laser Types: HPDL, Nd-YAG and CO_2 [4].

	HPDL	Nd-YAG	CO_2
Laser Power (kW)	< 10	< 4	< 40
Power Intensity (W/cm^2)	up to 10^6	up to 10^9	up to 10^8
Wavelength (nm)	790-980	1,060	10,600
Metal Absorption (%)	25-40	25-35	5-10
Efficiency (%)	25-40	3-5	10-15
Size of laser head (cm^3/W)	1	10	1000
Beam handling	Lens/Fiber	Fiber	Mirrors
Running Cost	Low	High	Middle
Capital Cost (CAD/W)	60-180	145-220	60-145

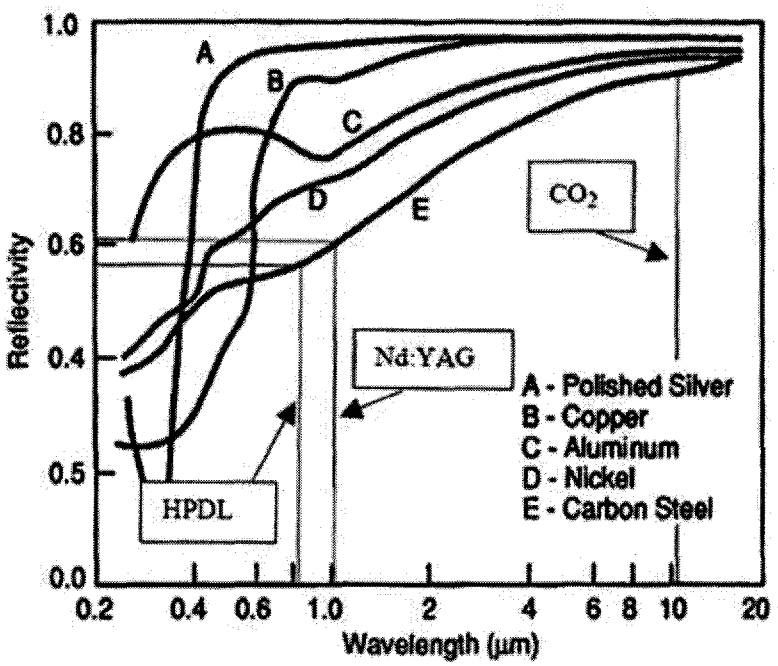

Figure 2.4: Reflectivity versus laser radiation wavelength for five metals [24].

Diode lasers work on the principle that when the electrons combine with holes in the depletion zone of a diode p-n junction, coherent laser light can be produced. A transparent semiconductor medium is thus required to transmit the laser beam. Typically a diode laser is constructed with InGaAs/GaAs semiconductor producing a 808 nm wavelength or from InGaAlAs/GaAs semiconductor producing a 940 nm

wavelength [25]. A single diode laser is comprised of just one p-n junction formed with two slabs of semiconductor material. Mirrors are placed at two ends of the diode to produce the Fabry-Perot lasing cavity. The resulting output power is only a few milliwatts emanated from a single diode laser with dimensions of only a few hundred microns [24, 26]. The output of a diode laser illustrated in Figure 2.6 has large divergence of up to 45° half angle perpendicular to the p-n junction emission line called the fast-axis while divergence is up to 10° half angle parallel to the emission line called the slow-axis [3].

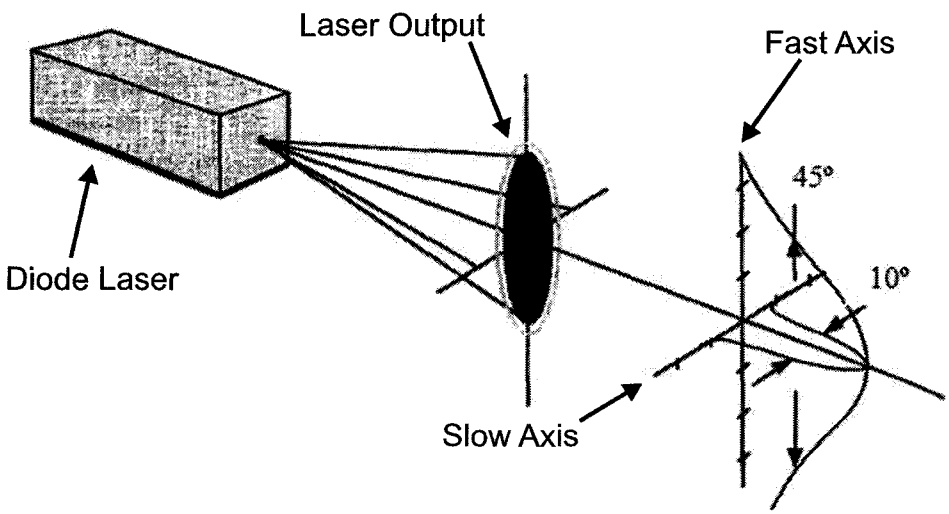

Figure 2.5: Output of a single HPDL laser stack showing the slow and fast axes [24].

Several diode lasers can be organized in a one-dimensional array about 10 cm long called a HPDL bar. HPDL bars allow increased power outputs of 30-50 W. The fast-axis of each bar is collimated by micro-lenses which are stacked on top of each other to form a diode laser stack producing powers of up to 1 kW as displayed in

Figure 2.6. Laser stacks can then be further combined to increase power levels. Laser light from the stacks are further collimated by a cylinder lens parallelizing the beam that is focused by a spherical photographic lens yielding a rectangular spot at the focal point of the laser. Theoretically, diode laser stacks can be continuously added for a limitless power output, however high levels of heat generated within the stacks must be dissipated and the size of the laser is limited by its cooling system.

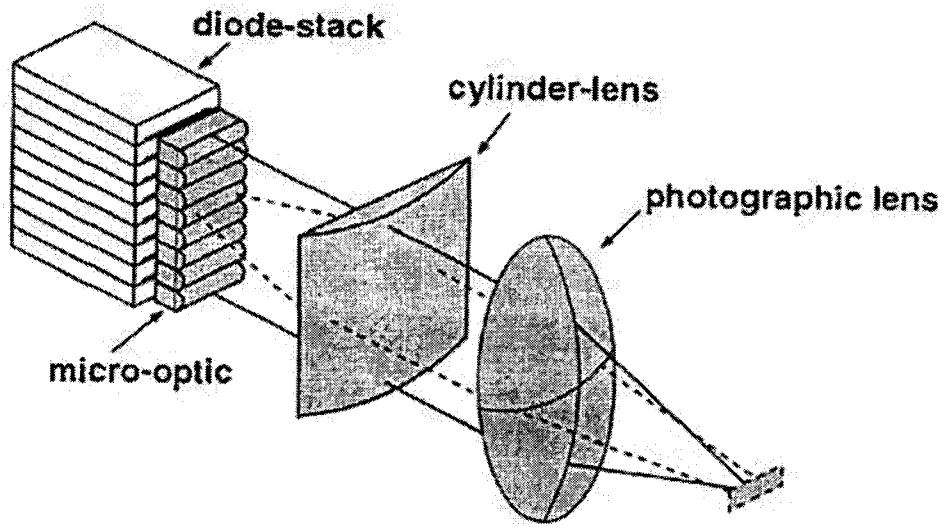

Figure 2.6: Focusing of light from a HPDL laser stack [4].

Unlike CO_2 lasers which require a complex systems of mirrors to transmit the beam, HPDLs can use fiber optics for beam transport, although this alters the spot shape from rectangular to circular. Electrical to optical conversion efficiency is greatly improved for a HPDL which is typically 20-30% and can be as high as 50%. CO_2 lasers have 10-15% efficiency while Nd-YAG efficiency is only 1-5% [3].

2.2.2 HPDL Surface Hardening

The combination of high efficiency, improved absorptivity, compact size, and rectangular spot shape make HPDLs ideal for surface hardening. The first report of laser surface hardening using a commercially available HPDL was by Klocke et al. [27]. Using a 650 W laser traveling with a 650 mm/min scanning speed, a hardened layer 0.4 mm deep and 4.5 mm wide was found when treating a 42CrMo4 steel workpiece.

A uniform hardened cross section with a hardness profile of up to 1.9 mm deep was found by Ehlers et al. [28] when hardening 4140 HT steel using a HPDL with a 22 mm beam width. A uniform track was found as a result of the homogeneous energy distribution of the laser beam. A second set of tests was performed using two HPDLs focused on a cylindrical workpiece. The two laser beams create a linear track 10 mm wide that covers 170° of the workpiece. A pyrometer was used to measure and control the hardened depth in-process. Hardened depths of 0.2 to 0.4 mm were found, however reported results and explanation were very limited.

Pantsar and Kujanpää [29] studied the effect of oxide layer growth when transformation hardening steels using a HPDL. Allowing an oxide layer to form by performing tests in air, absorptivity was shown to increase significantly when heat treating 42CrMo4 steel. Results illustrated in Figure 2.7 show an increase in absorptivity from approximately 40% in argon to approximately 53-73% in air. Absorptivity is also shown to increase for AISI 420 L stainless steel from approximately 38% in argon

to as much as 45% when treated in air. By measuring the surface temperature with a dual wave pyrometer the absorptivity was shown to increase with temperature in an oxidizing environment. It was suggested that a larger oxide layer is formed at higher surface temperatures which more readily absorbs laser radiation.

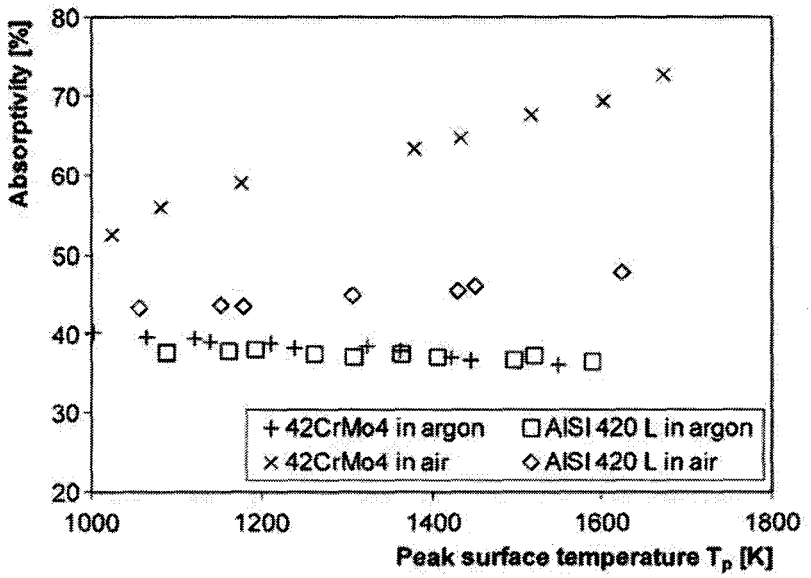

Figure 2.7: Effect of oxide layer and surface temperature on absorptivity [29].

A second study by Pantsar and Kujanpää [30] investigated the effect of workpiece surface finish on the laser-work absorption. The absorptivity was found through experiment by measuring the energy change using a liquid calorimeter. A 3 kW diode laser with a 12 x 5 mm hardening optic was used to treat a variety of prepared samples. The absorptivity was found to range from 46% to 72%. Figure 2.8a shows highest absorptivity for a workpiece with a graphite coated surface with little variation with scanning speed as oxidation has no effect on absorptivity. Machined and aluminum

oxide blasted surfaces are shown to have decreasing absorptivity with increasing scanning speeds. Figure 2.8b demonstrates increasing absorptivity with increasing peak surface temperature due to greater oxide formation.

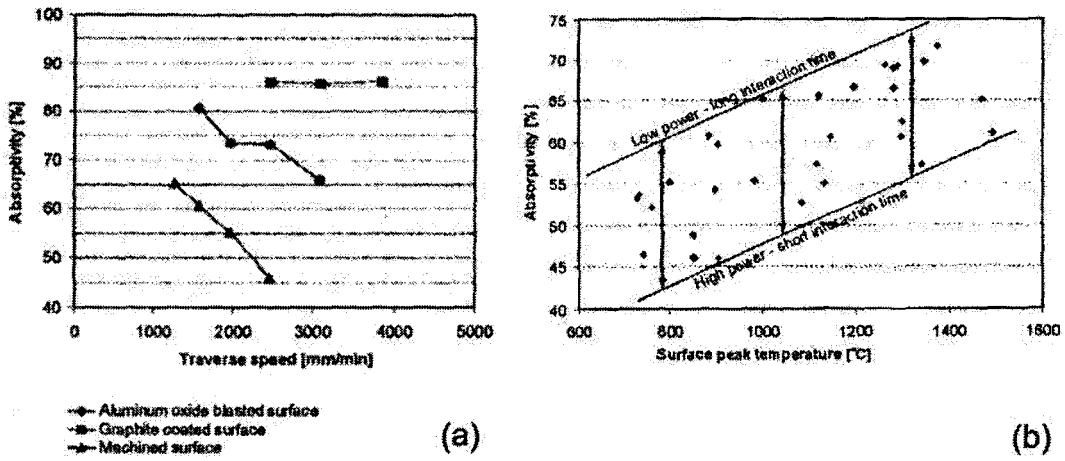

Figure 2.8: Effects of (a) surface finish and travese speed and (b) peak surface temperature on absorptivity [30].

Pashby et al. [31] used a 1.2 kW HPDL to treat a plain carbon (British Standard 080M40) and an alloy steel (817M40). Hardened depths up to 0.5 mm were reported for the alloy steel. The alloy steel showed the maximum hardening effect and hardness. Results summarized hardened depth and the existence of melting for set laser powers of 400-1000 W and scanning speeds of 50-1700 mm/min.

Heat treatment using a HPDL by Barnes et al. [32] was shown to be useful in the material processing of powder metallurgy (PM) components. The 1.2 kW diode laser with a 5 x 0.5 mm rectangular laser spot was shown to not only harden the components but also help seal surface porosity inherent with PM materials by re-melting. For high

scanning speeds the melted surface appeared smooth when viewed under a scanning electron microscope (SEM). Slower speeds resulted in a higher degree of melting and the resulting surface resembled that of a welding pass. Surface roughness was however increased from the as-sintered surface even for results at high scanning speeds (1500 mm/min) from 1.64 μm to 1.92 μm R_a respectively. The roughest result was that performed at low scanning speed (600 mm/min) and was measured at 3.39 μm R_a.

2.3 Modeling Laser Surface Hardening

The need for choosing appropriate process conditions lends itself to process modeling. As a result of the highly interdependent nature of the process conditions for laser hardening it is often necessary to describe temperature histories and phase transformations in order to predict the hardened case profile. An initial set of process conditions can then be acquired for an optimized process relating required case depth to laser power and scanning speed.

2.3.1 Temperature Modeling

Many analytical solutions for the heat diffusion into the workpiece have been developed. These solutions consider the workpiece to be a semi-infinite body with isotropic thermal properties independent of temperature. The laser radiation absorbed at the material surface is modeled as a constant moving heat source. The temperature field is considered quasi-steady-state meaning the temperature field changes

with time in respect to a fixed location on the workpiece, but remains steady with respect to the moving heat source. Solutions exist for moving heat sources modeled as an energy input at a point, line, circular and rectangle. The first of these solutions were those of Jaeger [33] and Rosenthal [34, 35]. Of these the simplest are the point and line source solutions. These are useful when the investigated temperature is at a location away from the source. Although when the temperature is desired at or near the source, temperatures are overestimated due to the heat flux integrated over an infinitely small distance. For this problem, a plane source can be used. Conveniently, plane source models exist that well approximate circular and rectangular laser spot geometry.

Rosenthal's moving analytical strip source model [35] consists of a heat strip which is the same length as the width of the workpiece. The workpiece is infinitely long and has finite width and height. The beam moves in the direction of the workpiece length parallel to the beam width. Essentially, the model is two-dimensional as there is no temperature gradient solved along the workpiece width. Rosenthal used his model to show the material heating and cooling time in welding.

Ashby and Easterling [36] used solutions to Rosenthal's equations of a point source to generate diagrams showing the extent of the heat effected zones in welding. However, the point source was not found adequate for describing the physical shape of the melt point or neighbouring isotherms. The problem was corrected by replacing

the point source with a circular disk [37, 38] with a Gaussian distribution. The model was mathematically the same as a point source solution; however, modification was made by offsetting the surface a distance below the 'model' surface with a correction factor. The limitation of this model is that it requires some calibration in order to determine an appropriate value for the correction factor. Modification by Shercliff and Ashby [39] was made to a line source as given by Rykalin [40] which is only useful when the scanning speed is high. Shercliff's et al. version adapted the model to a Gaussian plane source beneficial at all speeds. A non-Gaussian source was also shown possible by the superpositioning of numerous Gaussian sources.

Sandven [41] and Gregson [42] have developed simpler analytical solutions for one-dimensional transient heat flow, used for predicting the temperature distribution relative to the moving heat source. These solutions assume that heat flow is normal to the heated surface. Improvement can be found if modeled in three-dimensions. Cline and Anthony [43] as well as Sanders [44] developed a three-dimensional model for a semi-infinite plate under a Gaussian laser beam. Cline and Anthony [43] evaluated the model for use in heat treatment and welding with a scanning laser or electron beam. It was found that the model could be used for both applications without modification by neglecting latent heat effects due to melting and boiling. It was concluded that latent heat slightly alters the temperature distribution but has little influence on the penetration depth.

Chen and Lee [45] and Sanders [44], showed that the temperature rise produced by a scanning Gaussian round laser beam depends on the ratio of the scan speed and the materials thermal diffusivity as well as the ratio of the beam radius to the absorption depth. Sanders provides solutions for slow and fast scanning lasers. A critical velocity which is equal to the ratio of the diffusivity to beam radius [45] can be used to determine whether the temperature distribution can be modeled with a stationary heat source. The critical velocity for most semiconductors was found to have a value of 1 m/s.

Festa et al. [46, 47] developed simplified thermal models for the simulation of laser and electron beam surface hardening. The hardened depth and Peclet number is evaluated for one-dimensional stationary and a two-dimensional uniform scanning strip source. The hardness depth is reported in dimensionless form as a function of austenitization temperature. It was found that for Peclet numbers greater than 10 that the hardness depth could be evaluated with the one-dimensional model where the Peclet number is evaluated as the scanning speed multiplied by half the beam width over twice the thermal diffusivity. The investigation showed that the maximum hardening depth was limited by the occurrence of surface melting.

Kou and Sun [48] presented a two-dimensional heat flow model for the prediction of temperature distribution in cylindrical workpieces. Three cases were considered; heat source on the surface of a solid cylinder, heat source on the outer surface of a

hollow cylinder and a heat source on the inner surface of a hollow cylinder. The heat source shown in Figure 2.9a & b represented a laser beam reflected by toric mirrors that reflect the beam onto the workpiece in a continuous ring about the cylinder, while the workpiece passes through the stationary mirrors. The model then yields the temperature distribution radially and along the workpiece as illustrated in Figure 2.9c. The model was shown to compare reasonably well with experimental results for AISI 1018 steel.

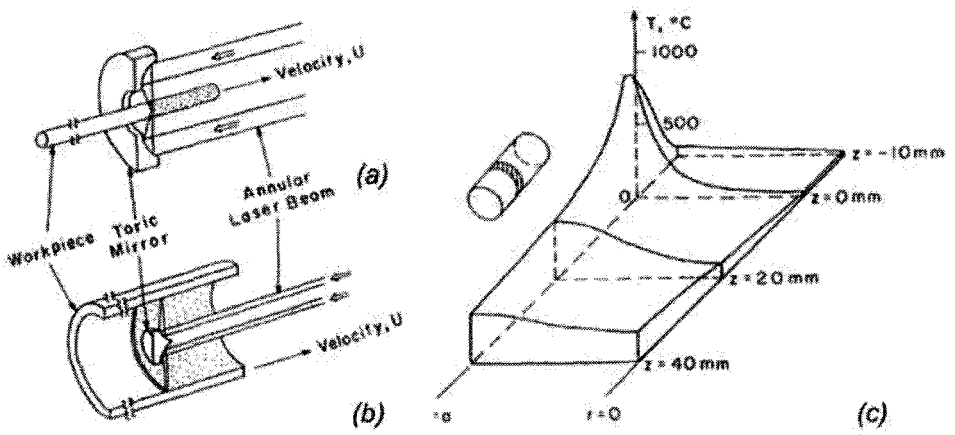

Figure 2.9: Laser hardening of cylindrical workpieces; (a) exterior hardening (b) interior hardening (c) temperature distribution [48].

The temperature field can also be solved by numerical integration. Lax [49] developed a one-dimensional integral for a stationary Gaussian laser source. Jaeger's [33, 50] three-dimensional moving rectangular heat source models a workpiece that is infinite in all directions, while the heat source however has finite size in both dimensions. This model yields a three-dimensional solution with temperature gradients along the length, width and height of the workpiece with respect to the heat source

center.

It has been shown by Tian et al. [51] that solutions to Jaeger's moving point source [50] can be modified by integration to obtain temperature solutions of different heat source distributions. Examples show solutions for circular and elliptical uniform heat sources. Hou and Komanduri [52] also reported modified versions of Jaeger's models comparing solutions of point sources to elliptical sources with uniform, parabolic and normal distributions. Rectangular, square and circular sources were also shown in the context of different manufacturing and tribological problems.

Komanduri and Hou [53, 54] provided a thermal analysis for laser surface hardening of AISI 1036 gear teeth pictured in Figure 2.10. The investigation compared uniform, Gaussian and bimodal beam shapes, stated by Mazumder [55] to affect the hardness distribution. Thermal analysis showed operating regions to maintain a 100 μm hardness depth without surface melting. Productivity was also examined as a function of beam size, shape and power, where the productivity was defined as the maximum surface area coverage rate yielding a 100 μm hardness depth. It was found that a beam with a uniform distribution was the most productive for any given beam size while a normally distributed beam was the least productive.

The simplest of all models are those that only calculate the maximum surface temperature. Kimura [56] and Meijer [57] found that even though laser hardening is primarily controlled by two independent process parameters, scanning speed and laser

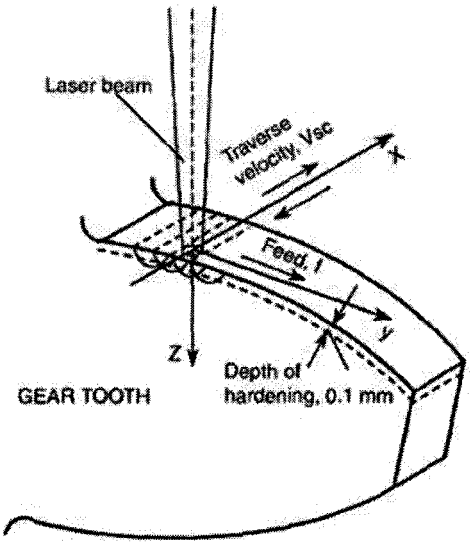

Figure 2.10: Laser hardening and thermal analysis of AISI 1036 steel gear teeth [54].

power, the hardness depth can be correlated to the maximum surface temperature. Meijer [57] points out the usefulness of this relationship by expressing that the surface temperature can be monitored and adaptive control strategies can be used to generate the desired hardness depth. However, Meijer's results were limited because constant absorptivity was assumed.

Although computationally more demanding, temperature distribution models solved by numerical integration can be currently solved within reasonable time. These models also allow for simulation of the spot shape and beam distribution. Finite difference and finite element models often require considerable computing power to obtain solutions but allow for greater flexibility than models solved by numerical integration. Such models can easily handle temperature dependent thermal properties as well as complex workpiece geometries.

Mazumder and Steen [58] developed a three-dimensional finite difference model of a moving circular Gaussian heat source along a rectangular slab workpiece infinite in length but with finite width and height. A convection heat transfer coefficient was added to simulate a concentric gas jet impinging on the upper surface that is used to shield the process during welding and heat treatment. The model was used to predict fusion, the heat affected zone and thermal cycles in the vicinity of the laser and to find the maximum welding speed. Model agreement was found reasonable when compared with the experimental work of Steen and Courtney [59].

An analytical model presented by Maier et al. [60] was solved by Green's function and finite difference methods. The model was used to investigate different beam shapes, single and multiple laser passes and pulsed laser treatment. Radiation and convective heat losses were investigated for multiple pass and pulsed laser simulation. Latent heat was neglected for phase changes as were temperature dependent material properties.

Chen et al. [61] also used Green's function to solve the temperature profile in a rectangular thin film due to a scanning uniform strip source. The solution was applied to a sheet of paper in an electro-photography process and it was found that the upper and lower surface temperatures were affected by the scanning speed, Gaussian radius and absorption depth. A criterion for the proper paper feed rate to avoid the paper from curling was also found.

Finite element (FE) modeling was used by Galantucci and Tricario [62] to model laser surface hardening of C40 carbon steel with a CO_2 laser modified to have an elliptical beam with a non-uniform energy distribution in order to simulate a diode laser. The study found that uneven energy distribution can cause uneven hardness distribution throughout the workpiece. It was also noted that FE modeling can be useful in process design for the determination of the dimension of the overlapping region of parallel laser tracks for prediction of the magnitude of remelting and heat affected back tempering.

Rajadhyaksha and Michaleris [63] compared the Lagrangian and Eulerian finite element formulations for laser hardening. Eulerian formulation can be used by taking advantage of the quasi-steady state nature of the temperature field in relation to the beam. Eulerian formulation can drastically reduce computer processing power when compared to Lagrangian formulation, which models the problem as completely transient.

Yanez et al. [64] used the combination of an analytical and FE model to investigate laser hardening of cylindrical A420 stainless steel pieces used in a multistage pump rotary jacket. The analytical model was found useful for its computational speed but the FE model was required to simulate overlapping as well as temperature dependent thermal properties and precise geometric effects.

2.3.2 Phase Transformation Modeling

Models have been developed to predict hardening of steel by laser heat treatment by either analytically modeling austenite formation and dissolution or by developing relationships through experiment. When combined with the temperature profiles calculated with a heat flow model the results give a prediction of the hardened case depth or hardened profile.

Ashby and Easterling [38] developed a kinetic model to predict hardness of plain carbon hypoeutectoid steels after laser treatment. The model calculates the kinetic strength for diffusion of carbon into austenite for pearlitic steels. It further expands the solution to include transformation of pearlite into austenite, the homogenization of carbon distribution within austenite and subsequent dissolution of austenite into martensite. Hardness was found from the volume fractions of martensite and ferrite. The phase transformation model was combined with results from a heat flow model simulating laser heating from a round laser source. Resolving a solution from the model required a number of difficult to find material properties, including pearlite plate spacing, carbon diffusion coefficient into ferrite and austenite and the activation energy of carbon into ferrite. A second model by Li et al. [65] extended the previous to include hypereutectoid steels, where an approximate solution for carbide dissolution was presented. The use of this model has been proven for plain carbon steels but does not include the effects of alloying elements in alloy steels.

Ion et al. [66, 67] used a similar model to Ashby et al. [38, 65] to show computed process diagrams including the change of the case depth and A_1/A_3 equilibrium temperatures with the laser traverse rate shown in Figure 2.11. The relationship was calculated with an analytical heat transfer and phase change model for idealized material properties. Changes in absorptivity and comparison with experiments were not shown.

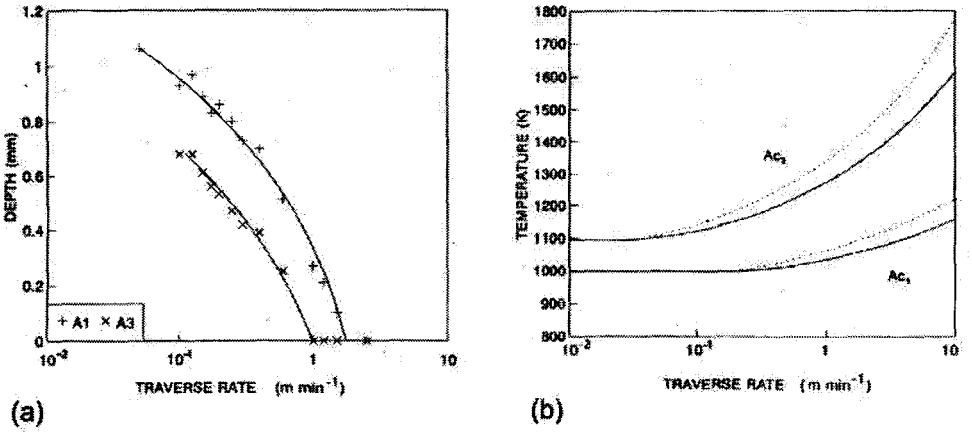

Figure 2.11: Computed diagrams for case depth and equilibrium temperature versus the laser scanning speed [67].

Ion et al. [68] reported a PC-based system for process development and prediction. Cooling effects were extended into the model for the formation of martensite, bainite and ferrite/pearlite mixture. Results were shown for a variety of alloy steels. Inputs required for the computer system included desired case depth, absorbed laser power, beam radius, and a first guess at the laser scanning speed to find the traverse rate. To find an estimated value of hardness the elemental material composition and the cooling time was required. Not reported were means to find the laser-work absorp-

tivity and the cooling time for scanning speed and hardness computation respectively. Further, the report did not indicate that rapid heating effects have a much greater effect on case depth for laser treatment than cooling rate, as previously shown.

De Pascale et el. [69] found good agreement between experimental measurements and predicted case depth of AISI 1045 steel under laser hardening with a 2 kW CO_2 laser. Prediction was found by finding the austenitizing depth from a heat flow model. The model assumes that full austenitization occurs in accordance with the iron-iron carbide phase diagram. Rapid heating effects were not shown in their results and experimental agreement was most likely found because of the very slow scanning speeds (< 15mm/s).

Meijer and Sprang [57] assumed that full austenitization can be assumed by shifting the equilibrium temperature reported on the phase diagram up to 910°C to account for rapid heating effects. Notably, 910°C is the austenitization temperature of pure iron. Combined with a heat flow model it was shown that peak surface temperature could be used to predict the resultant case depth. The model assumed a laser absorptivity of 56% for a CO_2 laser and no surface temperature measurements were performed to verify calculation with experiment. However, predicting case depth with surface temperature could prove useful for in-process inspection and control.

Analytical modeling is appropriate to help study the fundamental mechanisms in phase transformations. Consequently, analytical modeling of austenite formation

is useful only when the work material is ideal. Similarly, heat flow modeling can be tedious and time consuming. Without a good estimate for laser absorptivity the predictions given by the model can be highly inaccurate. For prediction of the size of the hardening layer, more practical methods should be developed that can be utilized for all steels and does not require in depth understanding of the physics behind the process.

For process improvement, laser absorptivity should be maximized, lowering the power output requirement of the laser and consequently lower the required capital investment. In order to study changes in absorptivity, an effective means of its measurement must be applied. Pantsar and Kujanpää [30] showed that the absorptivity can be measured with a liquid calorimeter. However, this requires complex equipment that cannot be easily implemented outside a research environment. A simpler technique that can be used with minimal equipment would allow for the absorptivity to be studied on the production floor.

Indicated by Meijer [57], in-process monitoring can be achieved by measuring the surface temperature at the laser spot. Meijer's results assume that the absorptivity is a known and unchanging value. It would be very useful to use an infrared thermometer to measure the surface temperature in order to monitor and control the resultant hardened layer without any knowledge or assumption of absorptivity.

CHAPTER 3
Experimental Details

3.1 Laser and Machine Tool

Hardening experiments were performed in a Nakamura-Tome SC450 turning center. The continuous beam laser system consists of the laser head, power supply, controller and cooling system. The laser head was mounted on the turret within the machine tool. Figure 3.1 shows the machine tool with the laser mounted on the turret and the laser power supply.

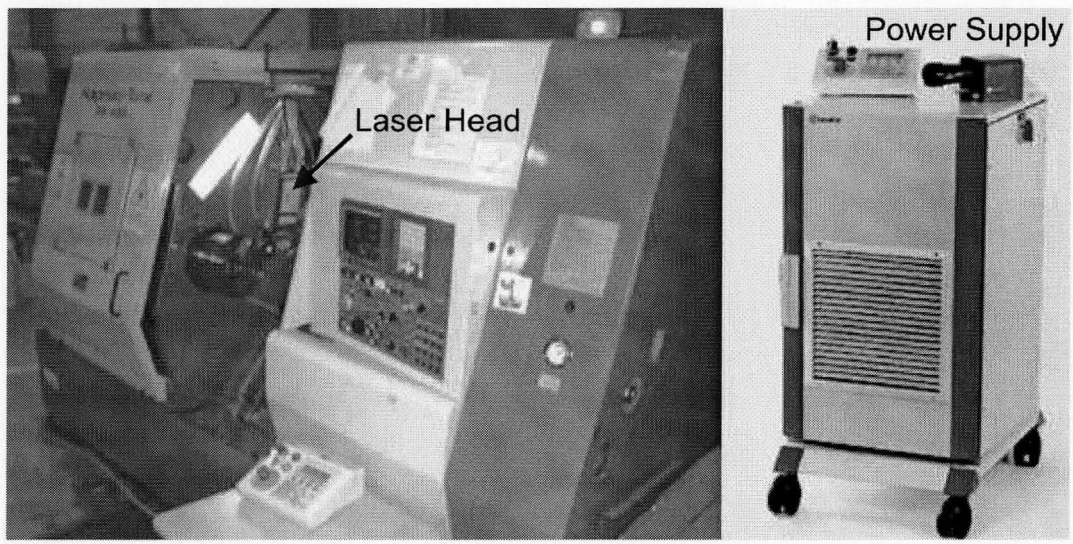

Figure 3.1: Laser in Machine Tool and Laser Power Supply.

Several safety modifications have been made to the laser/machine tool system to contain all reflected laser light within its construction. Experiments could be viewed through a small window made of laser safety filter glass, omitting the passage of harmful laser light of wavelengths within the range of 700-1200 nm. A door interlock

was in place to prevent the laser being turned on with the machine door open and would immediately shut the laser down if the door was to open. Cooling lines and electrical lines for the laser were brought into the machine through three black plastic elbows. The high power diode laser (HPDL) on its own has been categorized as a class four laser, however, with these modifications the system was revaluated as a class one laser system.

A Laserline GmbH 2kW high power diode laser model LDL80-2000 was used in all tests. Technical specifications are listed in Table 3.1. The rectangular spot size of the laser beam in focus is 4x0.9 mm^2, all tests were performed with the laser in focus, although defocusing the laser can allow for high surface coverage at a lower power density. The laser provides a low power pilot laser that is used for positioning and focusing using an infrared visualization card.

Table 3.1: Laser Specifications.

Maximum Laser Power	2000 W
Spot Size at Focal Point	4 x 0.9 mm Rectangular
Average Power Density at Focal Point	$5.6x10^6$ W/cm^2
Wavelength	808 nm - 940 nm
Beam Focal Point	85-90 mm from lens
Divergence Angle	20°
Laser Head Size	$410x150x130mm^3$

For ease of positioning and focusing of the laser, it was held in a fixture with six degrees of freedom assembled on the turret. The fixture allowed for the laser to translate and rotate about three orthogonal axes. The fixture also accommodated an

infrared thermometer to be placed on an articulating stand for precise positioning of the thermometer.

3.2 Workpiece Material

AISI 4140 or 42CrMo4 is a chromium molybdenum alloy steel, and was the workpiece material used for all tests. The material chemical composition given in Table 3.2 was in its annealed state with bulk hardness of approximately 207 Vickers (12.25 HRc extrapolated). The chromium provides this material with good hardness penetration while the molybdenum promotes uniform hardness. Thermal properties of AISI 4140 are listed in Table 3.3.

Table 3.2: AISI 4140 Chemical Composition (wt. %) [70].

C	Cr	Fe	Mn	Mo	P	S	Si
0.38-0.43	0.8-1.1	96.785-97.84	0.7-1	0.15-0.25	0.035 Max	0.04 Max	0.015-0.3

Table 3.3: AISI 4140 Thermal Properties [70].

Temperature (°C)	100	200	400	600
Density (kg/m^3)	7850			
Thermal Conductivity (W/m°C)	42.6	42.2	37.7	33
Specific Heat (J/kgK)		473	519	561
Coef. of Thermal Expansion (μm/m°C)	12.2		13.7	14.6

3.3 Hardening Configurations

Tests were divided up into three series of experiments: Slow, Fast and Double. The slow configuration consisted of twelve combinations of low power and low laser scanning speeds ranging from 200 to 1000 mm/min and 200 to 600 W laser operating

power. In these tests the laser scans along a linear path at the edge of a rectangular shaped workpiece as illustrated in Figure 3.2. The workpieces were machined to a 22 by 10 mm cross section and were approximately 200 mm in length. A round section at the end of the workpiece was machined in order for the workpiece to be held in the chuck of the turning center, which was kept stationary during this series of tests. All tests were performed with the laser angled 10° off perpendicular in the direction of travel to avoid harmful laser light reflecting back into the laser lens. The laser beam was held perpendicular in the axis orthogonal to the direction of travel.

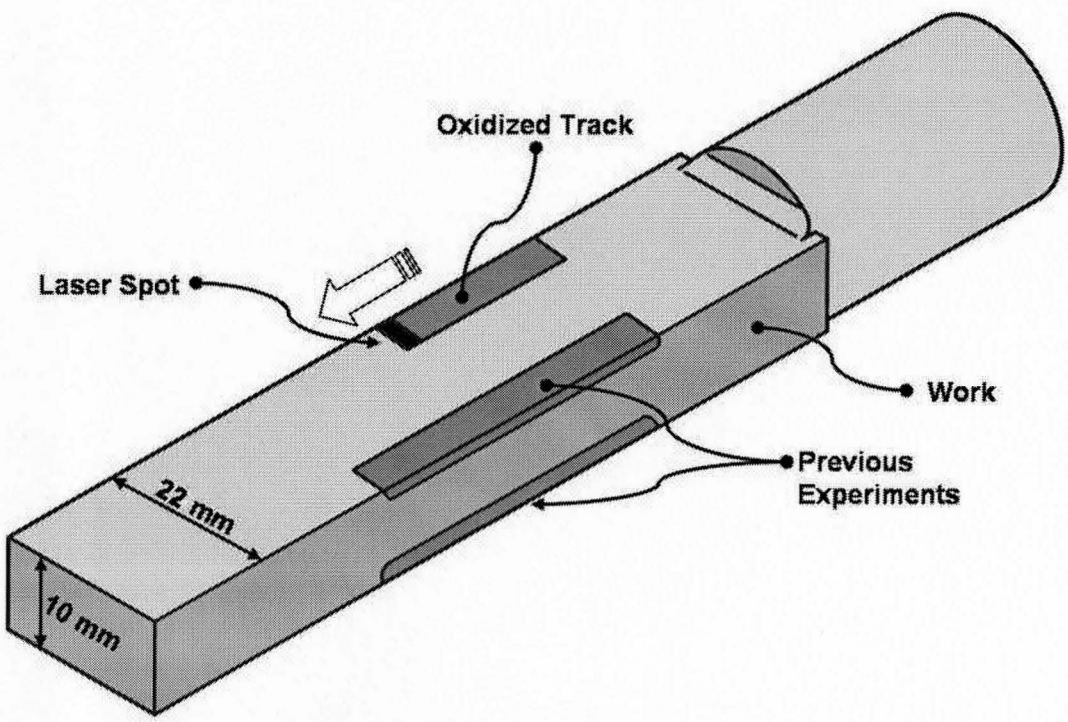

Figure 3.2: Slow Configuration, workpiece.

Separate tests were performed along each of the four corners of the workpiece. Melting was allowed to occur for some experiments, while oxidation was allowed to

occur for all experiments as this helped to increase the fraction of absorbed laser power. After hardening was complete samples were cut along the cross section of the work. Each sample contained a hardened zone at each of the four corners. Each hardened track was about 50 mm in length allowing for 3 sets of 4 experiments to be performed on each workpiece. Two samples were taken for each laser track yielding a total of 6 samples per workpiece. Samples were cut out downstream from the beginning of the track in the region where the temperature field could be considered quasi-steady. Sample cross sections were ground and polished with a 1 μm diamond suspension. Micro-indentation hardness measurements were taken 2 mm (half the width of the hardened track) from the edge of the sample and a micro-hardness profile from the surface into the workpiece was obtained.

Hardness testing was performed on an LECO M-400-H2 micro-indentation hardness tester equipped with a diamond indenter. All tests were done with a 100 g load, the two diagonals of the indent were measured corner to corner and ranged from 14 to 25 μm. The mean size of the indent diagonals was used to calculate the average hardness within the location of the indent. Algorithms within the hardness testing computer calculated hardness in both Vickers and HRc units. The sample was placed on an x/y table that measured the position of each indent on the workpiece.

Fast and double test series were performed at much higher scanning speeds than the slow test series. Fast tests consisted of one pass of the laser over the workpiece

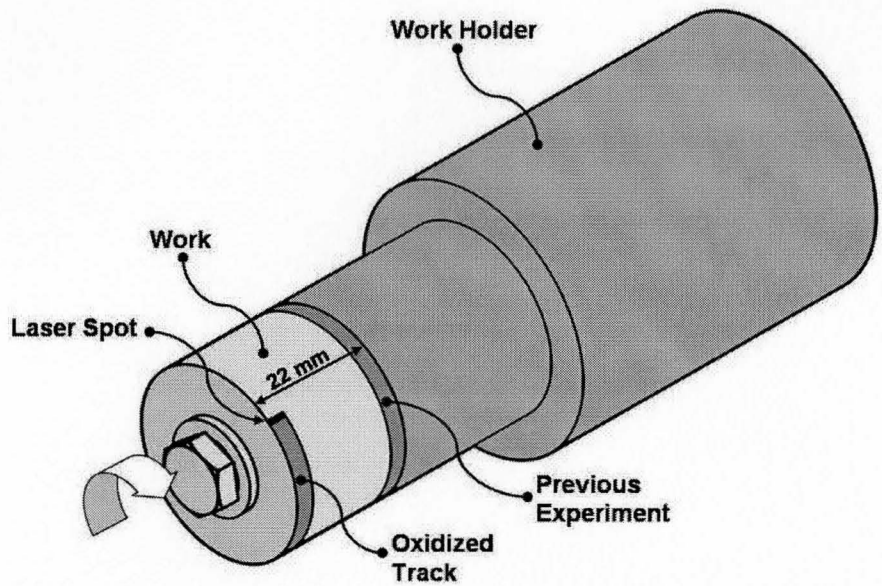

Figure 3.3: Fast Configuration, workpiece and work holder.

and double tests consisted of two passes in succession over the same region of the workpiece. Since it would take too long for the machine axis to accelerate to the scanning speeds performed in the fast and double experiments both series were performed on cylindrical workpieces 32 mm in diameter and 22 mm in width. Scanning speeds for both series of tests were in the range of 2000 to 8000 mm/min and laser power from 1000 to 2000 W. The cylindrical workpieces were held to a work holder by a single bolt. The work holder was then held in the chuck of the machine. Figure 3.3 shows a schematic of the workpiece and work holder. A test matrix for all tests is provided in Table 3.4 and both slow and fast/double experimental setups are shown in Figure 3.4.

As the fast series of tests consisted of one complete pass and the double series

Table 3.4: Experimental Parameters.

	Slow	Fast/Double
Laser Power (W)	200, 300, 400 & 500	1000, 1500 & 2000
Scanning Speed (mm/min)	200, 600 & 1000	2000, 4000, 6000 & 8000
Combinations Performed	All 12	All 24

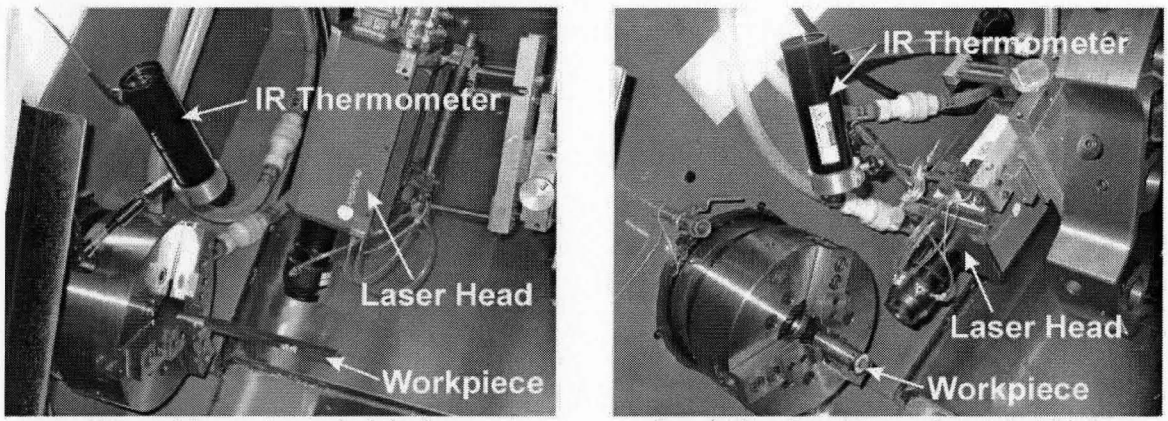

Figure 3.4: Experimental setup for both slow and fast/double configurations.

consisted of two passes. The laser was programmed for a single continuous pulse at the time period for one revolution for the fast series of experiments or two revolutions for the double series of experiments. The machine tool was then turned on and allowed to accelerate to its programmed rotational velocity. At this point the laser was turned on for the programmed time period and shut off automatically after the duration of the programmed time period. The angle of the laser beam was held 10° off center of the workpiece in the direction of rotation for all tests.

3.4 Temperature Measurements and Equipment

The greatest experimental challenge of this investigation was the temperature measurements. As a result of the extremely high temperature gradients ($\sim$ 800 to

1500 °C) within a very small area ($\sim$ 0.2 to 0.5 mm) present for only a fraction of a second ($\sim$ 0.05 to 0.5 s), specific temperature measurements proved difficult. As with many challenges faced with other means of measurement, reliable temperature measurements were finally achieved with thermally sensitive lacquers and an infrared thermometer.

OMEGALAQ temperature indicating lacquers shown in Figure 3.5 are applied to a surface in a thin coating. Once the lacquer is applied it dries almost instantly and forms an opaque film. As the lacquer reaches its response temperature it melts and changes appearance. The process is not reversible, therefore when cooled the previously melted lacquer does not return to its original opaque colour but appears glossy. The liquid temperature lacquers are available for many different response temperatures and are represented by different colours. The temperatures used in the performed experiments are outlined in Table 3.5. The thermal response time for the lacquers is on the order of 0.001 seconds and have an accuracy of 1.0 % as quoted by the manufacturer [71].

Table 3.5: Temperatures used for experiments [71].

Temperature (°C)	121	260	399	538	677	816
Colour	Purple	Light Blue	Green	Red	Grey	Dark Blue

The temperature lacquers were then applied in strips to the side of the work-piece next to the path of the laser. Several strips illustrated in Figure 3.6 were

Figure 3.5: Temperature Indicating Lacquer [71].

applied including 3 to 4 strips for each different temperature response. The resultant product after experiment left three regions. At the very top of each strip where the temperature was greatest the lacquer had vaporized and was no longer visible on the workpiece. The second region was the melt region which showed lacquer that had exceeded the response temperature and the third was the unaffected region. A distinct transition line apparent in most measurements between the melt and unaffected regions showed the depth at which the maximum temperature was equivalent to the response temperature of the corresponding lacquer. The distance between this transition line and the surface was measured with a tool maker's microscope. An example of temperature lacquers on a planar workpiece is shown in Figure 3.7.

Since the material was allowed to melt with some tests the remaining surface was often distorted. Measurements from the cross-sectioned samples taken for hardness testing were performed under the tool maker's microscope. Measurements were taken

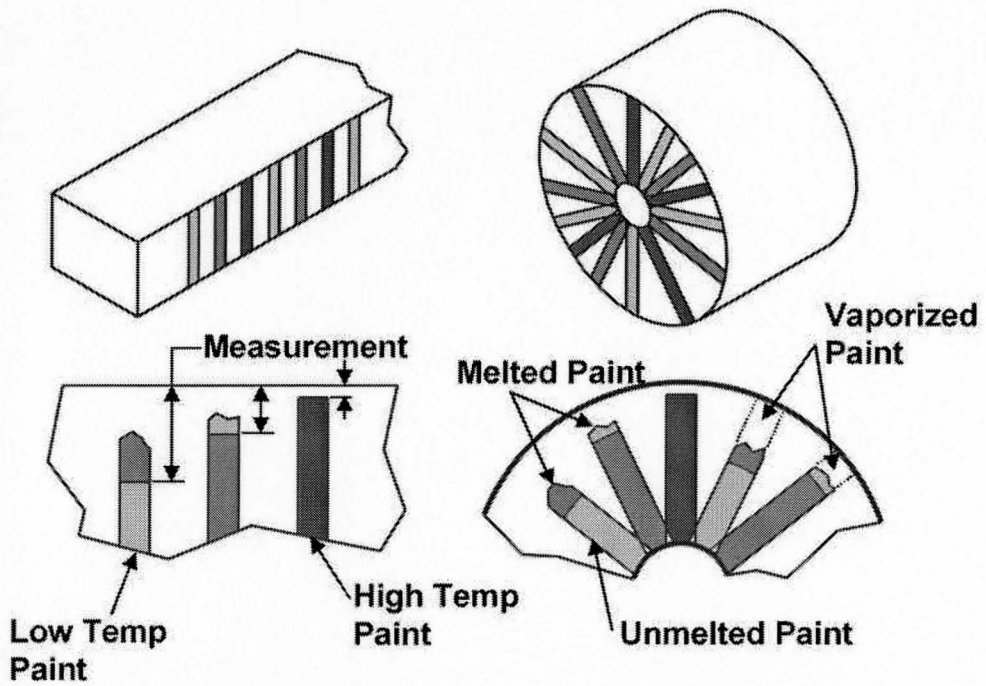

Figure 3.6: Measurement Procedure, left: slow configuration, right fast/double configuration.

of the new surface with the unaffected portion of the sample used as a reference line. The distances between the maximum height of deformed material above and below the reference was measured. The distance between the first hardness indent, the new corner and the reference line were also measured. These distortion measurements were used to adjust the hardness profile measurements and lacquer measurements for the corresponding sample.

A second means of temperature measurement was found with an infrared camera. The Raytek MASC infrared thermometer was used to take surface temperature measurements without any physical interaction with the workpiece. Table 3.6 lists the specifications of the thermometer. All tests were performed with the thermometer

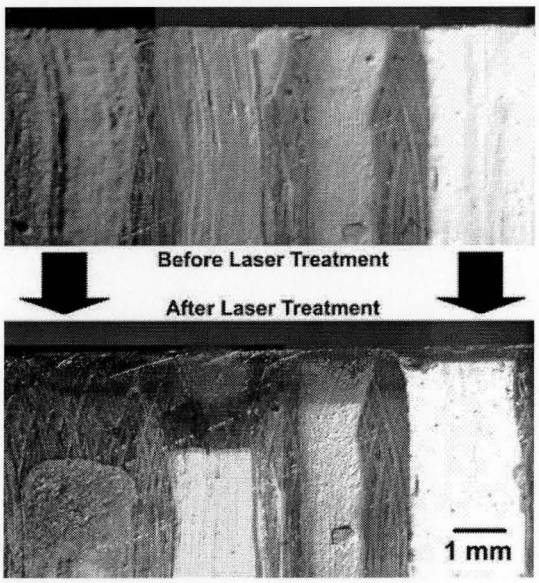

Figure 3.7: Temperature lacquers shown before and after laser treatment.

at its minimum focal distance for the minimal spot size of 1 mm. For the slow series of experiments the thermometer was held stationary with respect to the workpiece which captured the temperature change as the laser past through the focal spot. For the fast and double experiments the thermometer was held stationary with respect to the laser and could only capture the quasi-steady temperature at the focal spot. The thermometer was focused at the laser spot to measure peak surface temperature.

Table 3.6: Raytek MA2SC Infrared Thermometer Specifications.

Temperature Range	350 - 1400 °C
Nominal Spectral Response	1.6 μm
Detector	InGaAs
Accuracy	(0.30%Tmeas + 1 °C)
Repeatability	(0.10%Tmeas + 1 °C)
Temperature Resolution	1 °C
Fastest Response Time	1 ms
Emissivity Adjustment	0.10 to 1.0 in 0.01 increments
Focal Range	300 to 500 mm
Spot Size	Distance from measurement (mm) / 300
Spot Size at Min Focal Distance	1.0 mm dia

3.5 Experimental Limitations

Thermal lacquers were limited in that they could only measure the location which had a certain maximum temperature. Lacquers cannot measure the temperature as it changes with time. This was a limitation that had to be accepted as measurement methods that do not posses this limitation were found unreliable.

The infrared thermometer could however take time dependent measurements but was limited to readings above 350 °C. It also could not measure the variation of the quasi-steady temperature field for the fast and double tests as the thermometer had to be held fixed in position with respect to the laser spot. Furthermore, the fraction of emissive radiation cannot be found easily as it is critically dependent on temperature and surface condition. The measurements taken thus assumed the radiant emissivity of the workpiece to be 100%. Therefore, the infrared thermometer measurements do not represent the actual surface temperatures.

The largest variability is shown in the measurements of the lacquers themselves; because of heavy distortion as a result of melting with some tests the lacquer measurements are offset. Even though these measurements are corrected, they have a large variability of approximately ± 50 μm for the worst cases. To minimize the error the data was statistically fit to the results of an analytical model used to estimate the temperature distribution with respect to time and position and in most cases the error was minor.

CHAPTER 4
Results and Discussion

The benefits derived from integrating laser hardening within a machine tool structure has been corroborated through analysis and experiment. Results are presented and discussed in this chapter. To give evidence of the utility of this technology it was necessary to investigate the following:

- A method for determining the fraction of laser energy absorption is presented. Results were used to examine the effectiveness of the HPDL for heat treatment. Methods for increasing the absorptivity were found through the comparison of test results.

- A material hardness profile was measured for each test and was compared between results for slow (200-1000 mm/min) and fast (2000-8000 mm/min) scanning speeds, and for one or two laser passes. Strategies are presented that allow for easy initial process parameter selection for a given case depth.

- The minimum required finish machining depth after treatment was studied as this affects the final depth of the hardened zone.

- A method for in-process monitoring with the use of an infrared thermometer is discussed. The results indicated that infrared radiation can be used to observe

the process progress in real time.

- Temperature profiles were determined with the development of an analytical and finite element (FE) heat flow model, calibrated with the temperature indicating lacquer measurements. The model was used as an aid to determine absorptivity, yield predictions of case depth and relate temperature to measured results. Results are shown indicating differences between the analytical and finite element models.

4.1 Heat Flow Model

Two heat flow models were developed in order to calculate temperature distributions in the workpiece. The first is an analytical model adapted from Jaeger's [33, 50] moving heat source model to incorporate a Gaussian laser profile. The second is a finite element model built using the commercial FE solver ABAQUS. The analytical model is used for its simplicity and is compared to the more flexible FE model. The FE model can incorporate physical complexities such as geometry, temperature dependent thermal properties and surface heat losses.

Absorbed laser power and scanning speed are the governing parameters in both models. Material properties were chosen for those given for AISI 4140 steel [70]. In the next section the analytical model is used to investigate the fraction of absorbed power for different process parameters.

Figure 4.1 shows control volumes for the slow and fast/double test configurations. The primary energy input is the incident laser radiation which is distributed over the laser spot. However, only a fraction of the heat is absorbed by the work surface while the remainder is reflected away. The vast majority of the energy absorbed is conducted into the workpiece until the temperature gradient reduces to zero. A small amount of heat may be lost during laser heating at the boundaries of the workpiece in the form of convective and radiation heat transfer.

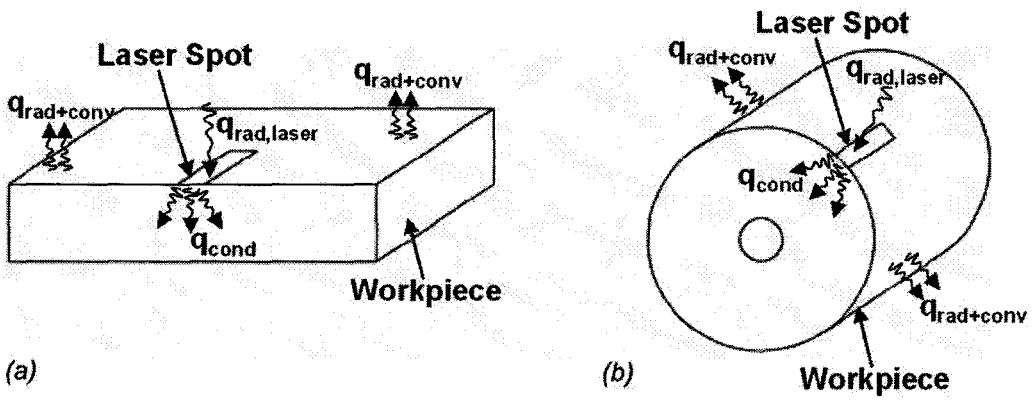

Figure 4.1: Process Energy Balance; (a) Slow and (b) Fast workpiece configurations.

The overall energy balance neglecting latent energy due to phase changes is given by equation 4.1:

$$q''_{rad,laser} - q''_{conv+rad} = \rho c \frac{\partial T}{\partial t} \tag{4.1}$$

where ρ is the workpiece density and c is the specific heat.

4.1.1 Analytical Model

The analytical model which requires significantly less computational time determines quasi-steady temperature profiles for a given heat source power and scanning rate. Laser heating during experimental runs was done along the edge of the workpiece as shown in Figure 4.1. Jaeger's solution however does not account for edge effects and assumes the workpiece to be semi-infinite in the +/- x, +/- y and + z directions as shown in Figure 4.2. To overcome this inconsistency a plane of symmetry is chosen at the edge of the workpiece and the length of the laser beam is doubled. The laser power is also doubled to maintain proper energy density. The plane of symmetry represents an adiabatic surface at the center of the beam where heat flows by conduction equally in both directions. In reality the plane of symmetry represents the side of the workpiece perpendicular and next to the laser scanning path. The comparison is justified if heat loss at this region is negligible. From Figure 4.2:

- V is the scanning speed of laser, (m/s)
- l is the actual length of the laser spot and the half length in the model, (0.004 m)
- w is half the width of the laser spot, (0.00045 m)
- and x,y,z are spatial coordinates originating at the center of the laser spot where negative x is in the direction of motion, (m)

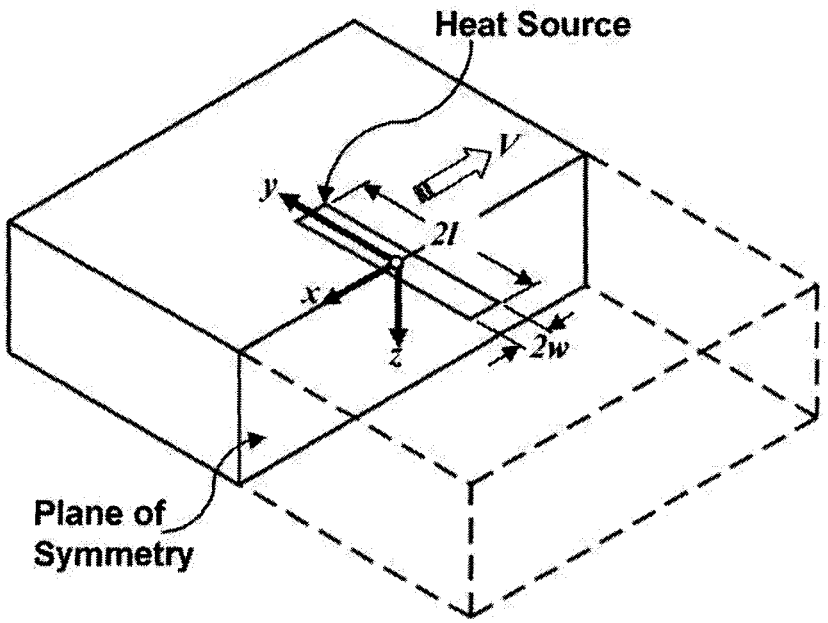

Figure 4.2: Jaeger's Moving Heat Source Model.

A solution to Jaeger moving rectangular heat source model [33, 50] given by Tian [51] is shown in equation 4.2.

$$T(x,y,z) - T_0 = \int_{-l}^{l}\int_{-w}^{w} \frac{q_0}{2\pi k s} \exp\left\{-\frac{V}{2\alpha}\left[s - (x - x')\right]\right\} dx'dy' \tag{4.2}$$

where:

$$s = \sqrt{(x-x')^2 + (y-y')^2 + z^2} \tag{4.3}$$

- α is the work thermal diffusivity, (m^2s^{-1}) given by:

$$\alpha = \frac{k}{\rho c} \tag{4.4}$$

- k is the material thermal conductivity, ($Wm^{-1}K^{-1}$)
- c is the material specific heat, ($Jkg^{-1}K^{-1}$)
- ρ is the material density, (kgm^{-3})
- T_0 is the initial work temperature, (K)
- q_0 is the absorbed laser heat flux, (Wm^{-2})

4.1.1.1 Beam Shape

The aforementioned solution for Jaeger's moving heat source model assumes the absorbed laser heat flux as a uniform input. The actual beam shape for the diode laser used in the experiments presented has a Gaussian distribution along the width and is uniform or top-hat along the length [24]. Figure 4.3 shows the Gaussian distribution of the laser spot along the width.

- q''_{max} is the maximum heat intensity located at the center of the beam, (Wm^{-2})
- q''_{min} is the minimum heat intensity located at the edge of the beam, (Wm^{-2}) and is given by:

$$q''_{min} = (1/e)\, q''_{max} \tag{4.5}$$

The general form of the equation of heat flux is given as a function of the distance from the center axis of the laser beam x and is shown in equation 4.6. This

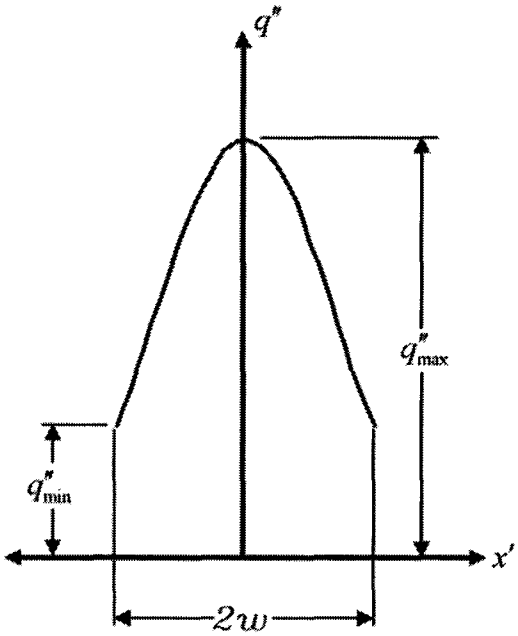

Figure 4.3: Gaussian Beam Profile

equation for heat flux is added into the integral solution for Jaeger's moving heat source.

$$q_0 = q''(x') = q''_{\max} \exp\left[-\left(\frac{x'}{w}\right)^2\right] \tag{4.6}$$

The maximum heat flux ($q''_{\max}$) can be found by integrating equation 4.6 over the spot area and setting it equal to the total laser power Q given in equation 4.7.

$$Q = 2\int_0^l \int_0^w q''_{\max} \exp\left[-\left(x'/w\right)^2\right] dx'dy' \tag{4.7}$$

By integration:

$$q''_{\max} = \frac{Q}{2\sqrt{\pi} \cdot wl \cdot \text{erf}(1)} \tag{4.8}$$

where:

- Q is the total absorbed laser power, (W)
- erf(1) is the Gaussian error function of $1 \sim 0.8427$

The analytical solution is then solved by numerical integration to calculate temperature profiles in three-dimensions. This model cannot however resolve a solution including temperature dependent thermal properties or include heat losses from the workpiece. The model also simulates a semi-infinite workpiece where temperature build-up due to finite geometry is not considered and may cause disagreement from experiment.

4.1.2 Finite Element Modeling

A transient heat transfer finite element model was built in the commercial FE solver, ABAQUS. The model was built using three-dimensional 8-node heat transfer elements. The beam shape and motion were defined by writing a FORTRAN user subroutine which ran parallel to the FE solver. The model was used to study the effect of adding physical complexities not included in Jaeger's analytical solution. The two complexities considered were:

1. Temperature dependent thermal properties.

2. Heat loss at the work surface by radiation.

The workpiece in the FE model was built with the same cross-sectional dimensions as a workpiece used for the slow series of experiments. Geometrical effects were shown to be negligible since there was no heat build-up on the workpiece at regions away from the laser/work interaction zone for the time period the model was run.

4.1.2.1 Element Size and Time Step

The element size on the laser/work interaction surface and the length of each time increment had to be chosen carefully. It was determined that the element size should be chosen such that the laser spot size would be an integer multiple of this value. The position of the laser spot was aligned with the FE mesh so that there were nodes coincident with the edges of the laser spot. The time step was also chosen such that alignment was maintained from increment to increment while the laser spot is moving. If these conditions were not met, a fraction of the intended input heat flux would not be captured by the model.

Figure 4.4a illustrates a situation where the element size was not appropriately chosen so that the edges of the spot are not coincident with any nodes that would, result in an erroneous computation. Figure 4.4b shows a situation where the laser beam is aligned such that most of the incident power was captured by the model; only a small amount was lost as a result of linearization of the Gaussian heat flux profile between nodes, which could be minimized by reducing the element size.

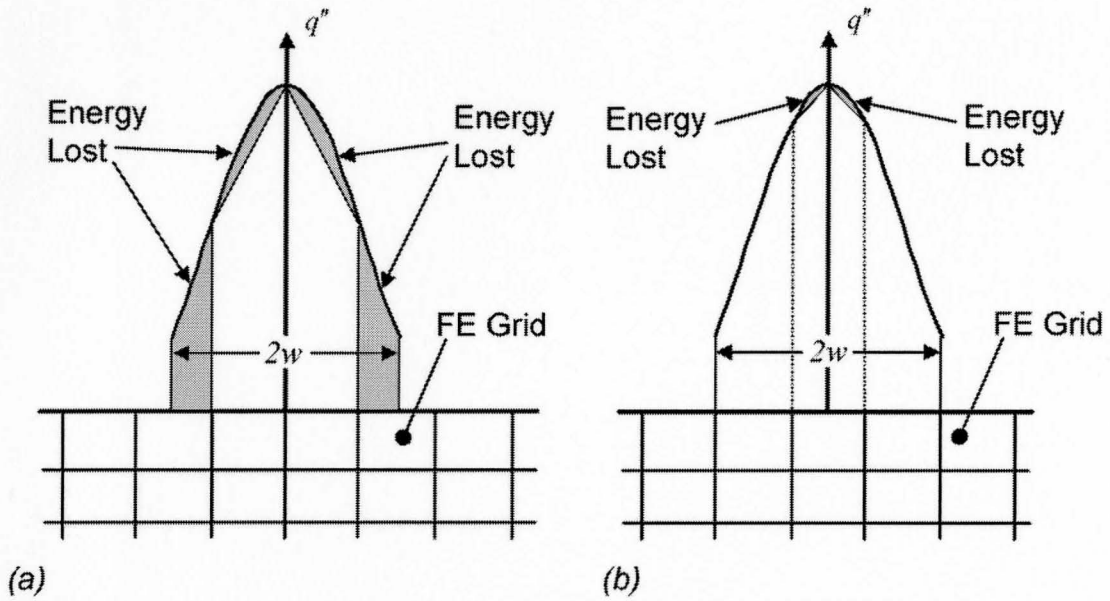

Figure 4.4: Beam orientation with finite element mesh, (a) Aligned beam orientation with improper element size, (b) Centered beam orientation with appropriate element size.

The two orientations, depending on whether the number of elements within the laser spot is even or odd and is defined as:

Aligned: There is an even number of elements within the laser spot so that the center of the spot is coincident with the central node (see Figure 4.4a).

Centered: There is an odd number of elements within the laser spot so the center of the spot is positioned midway between two nodes (see Figure 4.4b).

The error invovled when the element size and time step are not chosen carefully can be significant. By reducing the element size the error will eventually decrease and become negligible although the computer power required to process the model will increase exponentially. Figure 4.5 shows the power loss for the number of elements

under the laser spot for aligned and centered orientations. The greatest power loss is observed when the number of elements under the laser spot is slightly less than the nearest whole number, since the edges of the laser spot are furthest away from the nearest inner node in this condition. It is evident that the power loss decreases with the element size, however smaller elements are computationally more demanding as more elements are required to fill the workpiece volume. The need for a small element size can be minimized by maintaining an aligned or centered orientation with proper element size, greatly increasing the efficiency of the model.

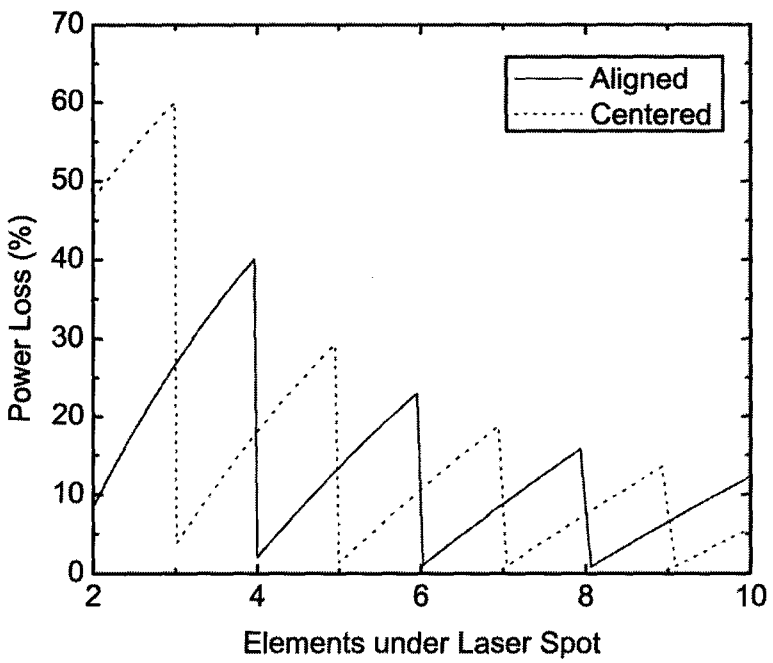

Figure 4.5: Power loss as a result of the number of elements within the laser spot for aligned and centered beam orientations.

4.1.2.2 Finite Element versus Analytical Modeling

A wide variety of publications exist regarding analytical and finite element models each representing varying levels of complexity. However, the need for developing complex models that consider many of the physical realities involved in laser heating has not been addressed in the literature. The following is a brief comparison of the effect of adding temperature dependent thermal properties and surface heat losses due to radiation and convection which are very difficult to incorporate into an analytical model. This serves as an assessment of the need for finite element modeling in order to include these factors at the expense of the small calculation times associated with an analytical solution.

Temperature dependent thermal properties can be easily incorporated into a finite element model. Reported values for thermal material properties below 100 °C and above 600 °C were not found and are assumed constant outside this range. Problems can also arise if any erratic changes in the thermal properties data exhibit significant non-linearity. For the purpose of this study the thermal properties used have been adapted from Table 3.3 and are summarized in Table 4.1. Temperature independent models used thermal properties related to the lowest temperature indicated.

Results shown in Figure 4.6 compare the results of the Jaeger's moving heat source model with the finite element model for both temperature dependent and independent thermal conductivity and specific heat. Temperature profiles are shown

Table 4.1: Temperature dependent thermal properties adapted from ref. [70].

Thermal conductivity (W/mK)	42.6	for T <= 100 °C
	-0.019T + 44.5 33	for 100 < T < 600 °C
	33	for T >= 600 °C
Specific heat (J/kgK)	473	T <= 200 °C
	0.22T + 429 561	for 200 < T < 600 °C
	561	for T >= 600 °C

for a location on the workpiece at the surface and at 0.5 mm below. Both locations are situated on the plane of symmetry at the centerline of the laser track. The finite element model estimates a higher maximum surface temperature than Jaeger's model in both circumstances. Temperatures away from the maximum are nearly identical for all cases at both the surface and 0.5 mm depth. The maximum temperature at locations below the surface was found to have little difference between cases as is shown in Figure 4.6b.

Therefore, it is evident that the inclusion of temperature dependent thermal properties in a FE model is only necessary if a more accurate calculation of the maximum surface temperature is required. It is unclear whether a temperature independent finite element model yields a better estimate of the maximum surface temperature than Jaeger's solution. As no exact surface temperature measurement is available it cannot be concluded which model's estimate is closer to reality.

In order to include surface heat losses in the FE model, thermal radiation was added through a user subroutine. The rate of energy loss for each surface node was calculated from equation 4.9 for every time increment.

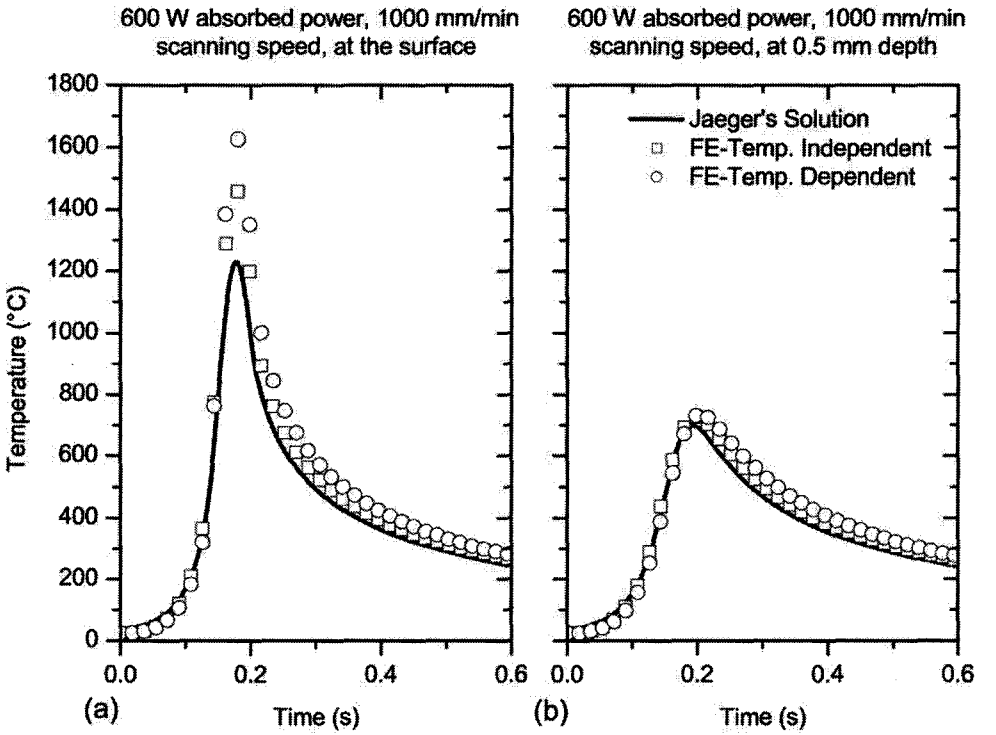

Figure 4.6: Comparison of Jaeger's model and finite element models including both temperature independent and dependent thermal properties, at (a) the surface and (b) 0.5 mm depth.

$$q'' = q''_{rad} = \sigma\varepsilon(T_N^4 - T_\infty^4) \tag{4.9}$$

where:

- T_N is the nodal temperature, (°C)
- T_∞ is the ambient air temperature, (°C)
- σ is the Stefan-Boltzmann constant, ($5.67\text{x}10^{-8}$ $\text{Wm}^{-2}\text{K}^{-4}$)
- ε is the total radiative emissivity which was evaluated from relationships derived from tabulated emissivity values for polished mild steel [72].

Convection, on the other hand, has been neglected in the investigation as it is assumed to only have influence on the temperature profiles in the long term as this is the primary mode of heat transfer out of the workpiece. The insignificance of convection in the short term can be explained by examination of the temperature profile which shows a very small heated surface region with respect to the entire workpiece surface. Such a small ratio cannot have the driving force required to create buoyant induced fluid motion which results in comparable convective heat flow with respect to the input energy from the laser beam.

Heat loss effect due to surface radiation is shown in Figure 4.7 and is compared with models that do not include heat losses. It is evident that the heat loss effect has negligible influence on the temperature profiles on the surface or below. Radiation heat loss effects have therefore been neglected in further calculations.

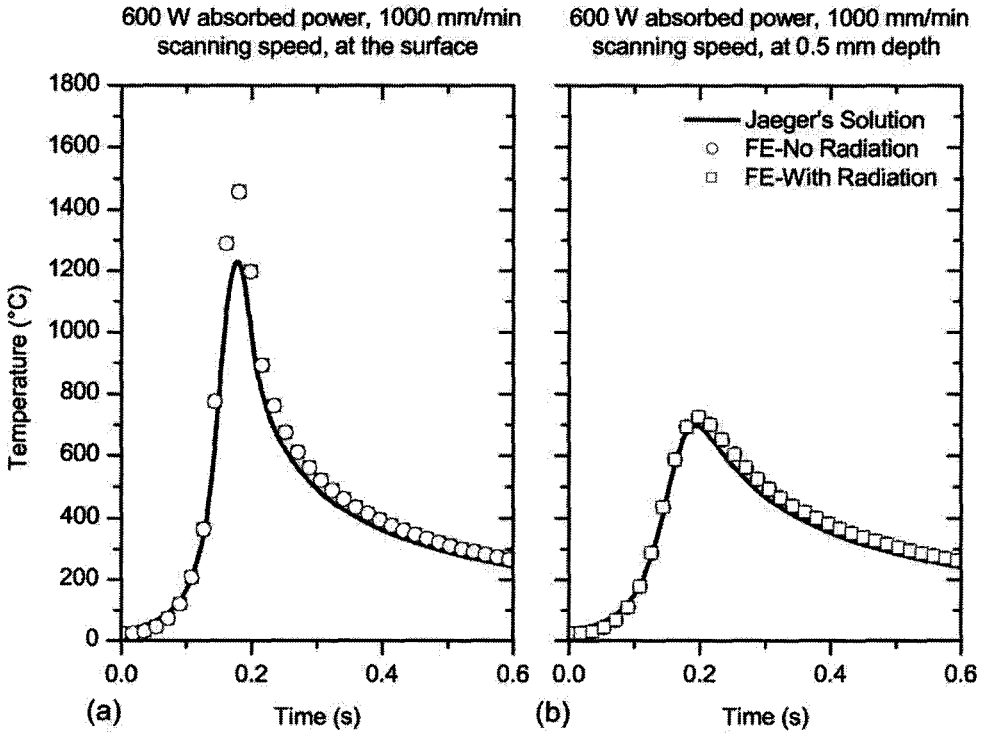

Figure 4.7: Temperature profiles comparing Jaeger's model and finite element models including and not including heat losses at the work surface due to radiation, at (a) the surface and (b) 0.5 mm depth.

4.2 Absorptivity Measurement

Absorptivity is defined as the fraction of laser energy absorbed by the workpiece material. It is dependent on many factors including laser wavelength, workpiece surface finish, material type and surface temperature. Many researchers have considered absorptivity to be constant in order to simplify their investigations. As will be shown in this study absorptivity is a key variable and the assumption of its constancy is not valid. Increasing laser absorptivity can reduce capital costs of the laser as a lower power laser may be found sufficient for a certain application. Higher absorptivity will also increase heat penetration resulting in a larger hardened surface layer for a given

incident laser energy.

Measurement of absorptivity is a difficult task. Previous methods have proved challenging to employ. Liquid calorimeters have been used to measure the absorbed laser energy of a single workpiece by submerging the workpiece after treatment into a liquid. The temperature increase of the liquid is recorded until uniform with the workpiece. The energy input is then calculated using the first law of thermodynamics. Although, this method is accurate and theoretically simple, it can be difficult to implement in many experimental setups since it is necessary to submerge the workpiece into a liquid bath quickly and consistently. The bath must also be fully contained within an insulated container with a sealing lid.

Thermocouples have also been used to measure the temperature change with time at specific locations on the workpiece. The measurements are compared with calculations from a model which has an absorbed power input that agrees the best. A benefit of thermocouples is they can measure the temperature change with time at a given location. Unfortunately most thermocouples have too low a response time for laser heating. High thermal inertia and poor contact conductivity inhibit the thermocouples ability to change temperature at the same rate as the workpiece. The contact area can also be large resulting in average temperatures that do not well represent the temperature profile.

Infrared thermometers have been used to measure the surface temperature of a

workpiece. This method is advantageous since no surface contact is required and it has no thermal inertia. Conversely, the readings are highly dependent on the surface spectral emissivity which can vary depending on temperature. The thermometer can be calibrated for emissivity but requires a second method of temperature measurement. Furnace heating can be used to raise the workpiece to a known temperature although this does not well represent rapid laser heating with its steep temperature gradients and surface oxidation.

A novel approach has hence been developed for absorptivity measurement in this study. Temperature sensitive lacquers are used to indicate depths at which the maximum temperature is equal to the indicating temperature of the lacquer. Several measurements were taken for different lacquers representing different temperatures. The maximum temperature versus depth curve was calculated numerically from Jaeger's moving heat source model for a range of absorbed laser powers. The calculated curve with the absorbed laser power that minimized the total of the residuals between this curve and the measured data was used to estimate the absorptivity. Figure 4.8 shows two best fit solutions for the temperature indicating lacquer measurements.

The second pass of the double pass test series was calculated from Jaeger's model by finding the average radial temperature after one workpiece revolution with the laser on. The radial temperature distribution at this point is found by using Jaeger's model with the absorptivities calculated from the fast series of tests as they represent the

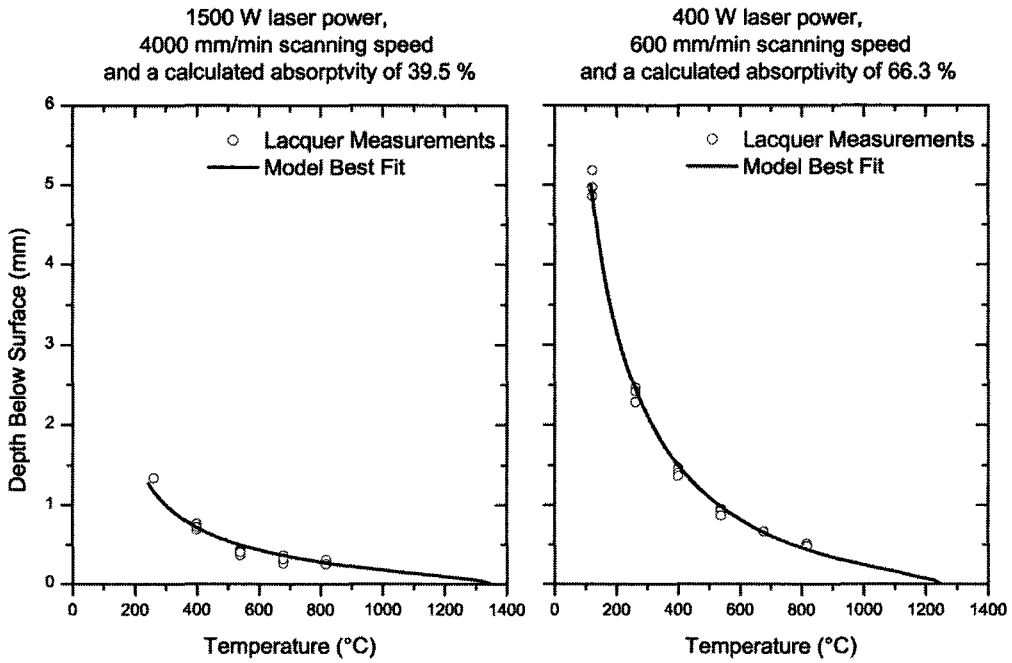

Figure 4.8: Best fit model solutions for temperature indicating lacquer measurements.

first pass of the double pass series. The temperature gradient just prior to the second pass is insignificant as heat has by then been uniformly distributed throughout the work material. The convergence of the temperature profiles at different depths solved by an FE model simulating a cylindrical workpiece can be seen in Figure 4.9. The results shows the temperature profiles for two laser passes.

The average temperature calculated after the first pass is used as the initial work temperature in the analytical model. The model was run until a good fit to the lacquer measurements taken for double pass series of tests was found. This method was compared with results from the cylindrical workpiece finite element model undergoing two rotations with a stationary heat source. Figure 4.10 compares Jaeger's model results to the finite element results for the penetration depth as a function of peak

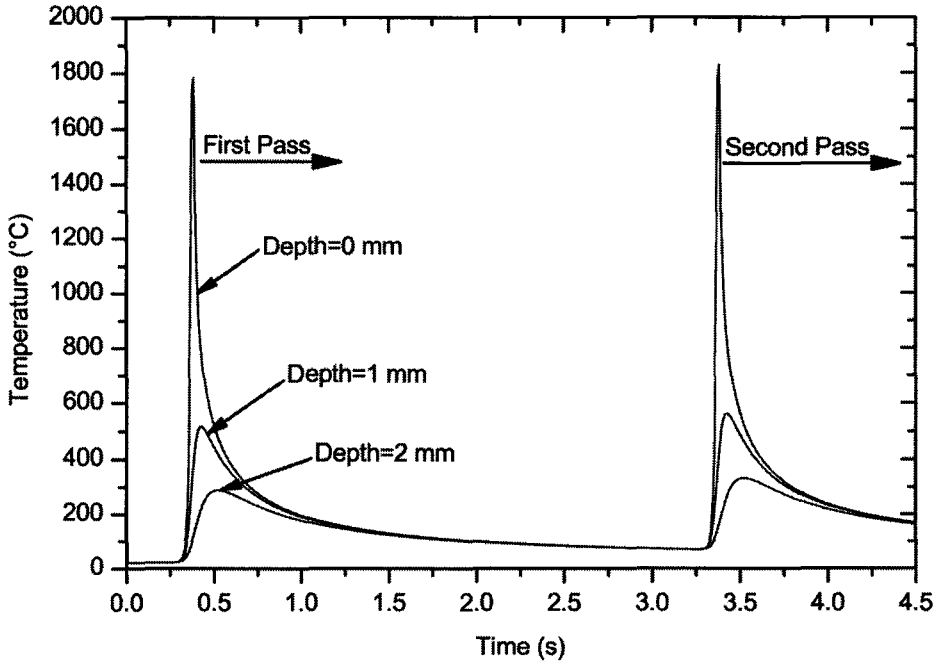

Figure 4.9: Temperature profiles from FE method at 0, 1 and 2 mm from the surface for two laser passes with 500 W of absorbed power and 2000 mm/min scanning speed.

temperature for the second rotation. Jaeger's model was then used in this way as before with the lacquer measurements to calculate absorptivity.

Figure 4.11 shows a range of laser absorptivities for all experiments ranging from 30 to 85%. Highest absorptivity realized in all experiments was approximately 80%. The typical absorptivity of a CO_2 laser beam for a low alloy steel ranges from 4.5 to 11% [30]. To increase the absorptivity of a CO_2 laser on a metallic surface a non-reflective coating must be applied. Such a coating was not required to achieve good absorptivity with a HPDL laser. The shorter wavelengths of the HPDL are more easily absorbed by a metallic material.

Figure 4.11 shows an increase in absorptivity for all test series when there is

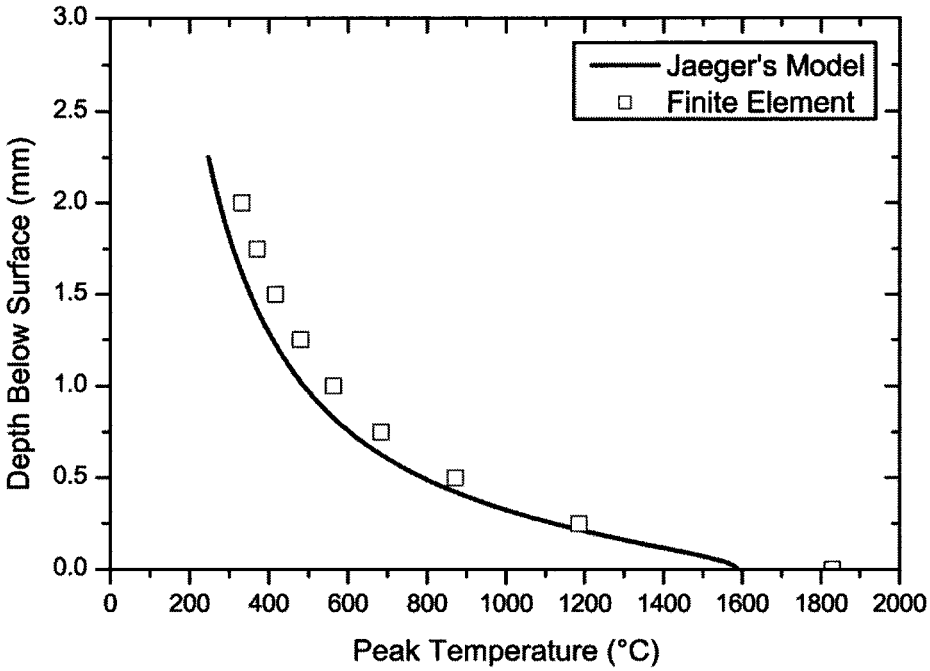

Figure 4.10: Comparison of Jaeger's moving heat source model with adjusted initial temperature to finite element model, for two laser passes with 500 W of absorbed power and 2000 mm/min scanning speed.

a decrease of laser power. The range bars indicate the standard deviations between calculations for each test with a single repeat. A minor increase is also observed for an increase in laser speed for the two high speed cases. No significant change is noticed for the slow speed case. Highest absorptivity was apparent in the slow speed tests.

Figure 4.12 shows a decrease in absorptivity with increasing maximum surface temperature for the slow and fast scanning speed tests. Overall, the slow tests show higher absorptivity regardless of surface temperature. The difference could be a combination of two factors: The most obvious is that the slower scanning speeds allowed for additional absorption time and the second may be related to the material surface finish. A milling operation was used to produce the surfaces on the flat workpieces,

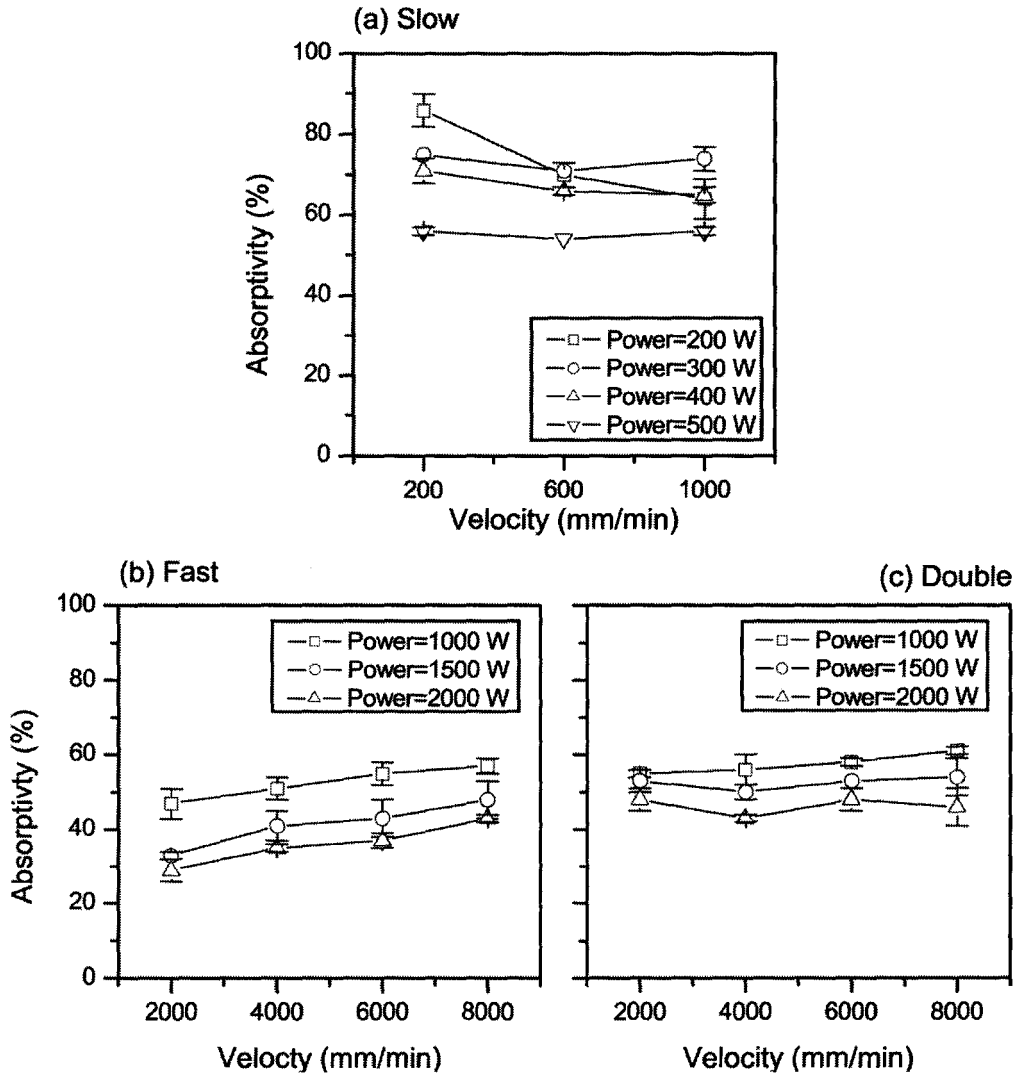

Figure 4.11: Calculated absorptivities for (a) (Slow tests) slow scanning speeds and low laser power; (b) (Fast) first pass and (c) (Double) second pass at fast scanning speeds and high laser power.

which were used for the slow tests. This generated a much different surface than the turned cylindrical workpieces that were used for the fast tests. The measured roughnesses were ~ 2.7 and ~ 3.9 μm R_z for the flat and cylindrical workpieces respectively. However, traditional roughness measurements do not fully characterize the surface topography and cannot be used to make definitive conclusions. Laser ab-

sorptivity has been proven to be very dependent on the surface finish [30] and so the two test sets cannot be directly compared. Workpiece curvature on the cylindrical workpiece may increase the reflectivity of the laser beam as the incident beam angle may be increased due to the curvature. This effect is suspected to be small as the laser is aligned so that the workpiece curvature is along the laser spot width which is only 0.9 mm.

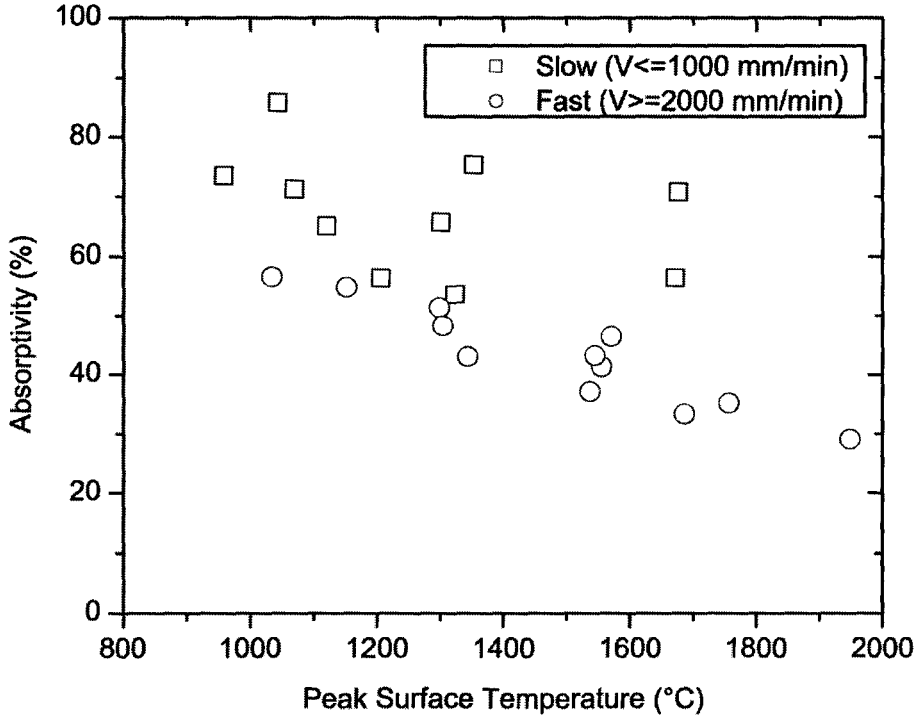

Figure 4.12: Calculated absorptivity shown against the calculated maximum surface temperature for the first pass at fast scanning speeds and high laser power.

Surface temperature tends to have an decreasing trend on the absorptivity, as is most noticeable for the results of the fast series of tests (Figure 4.12). This trend does not however agree with the findings of Pantsar and Kujanpaa [29, 30] as the opposite

was found from liquid calorimetric measurements. It is suggested that the higher surface temperatures produces a thicker oxide layer that can absorb laser energy more readily [29].

It is suspected that the surface finish plays a key role in the absorption of laser energy. The prior machined surfaces consisted of many peaks and valleys generated during machining. As suggested by Pantsar and Kujanpaa [30], this topography reflects a fraction of unabsorbed laser radiation back onto the work surface and therefore increases absorptivity. After the point of melting a weld pool begins to form and the surface topography becomes smooth, the absorbing benefits of the machined surface are no longer realized. The decreasing trend found by Pantsar and Kujanpaa was for experiments that did not exceed the melting temperature.

Large variation in both Figure 4.12 and Pantsar and Kujanpaa's results prevent conclusions about the actual trend of absorptivity with surface temperature from being drawn. More work is needed to study the physical mechanisms in greater detail to determine the allowable absorbed laser radiation.

4.3 Penetration Depth of Fully Transformed Phases

A hardened material surface profile depends on the depth at which significant material transformation occurs so that after heating and cooling a hard martensitic microstructure is left near the surface. The maximum possible thickness of the martensitic layer or hardening case depends on the penetration depth of the heat

conducted into the workpiece. Locations that have reached the critical transformation temperature (A_3 line from the iron-iron carbide phase diagram) begin to form austenite. However, due to rapid heating effects the equilibrium temperature can be shifted above the A_3 line. A reported [57] heuristic is that medium to high carbon steels that have surpassed 910 °C when undergoing rapid heat treatment can be assumed to be fully austenitized. Predicted case depths were made from this criterion by using Jaeger's heat source model with the previously found absorptivities.

Case depth readings were found from micro indentation hardness measurements. As discussed by Klaren et al. [73] a threshold value of 50 HRc is used to define case depth. The case depth is the distance from the original surface prior to heat treatment and the final hardness reading above 50 HRc before the hardness profile drops to the base material hardness. The hardness criterion of 50 HRc is arbitrary, and can vary as may be desired. For this report 50 HRc was chosen as all measurements between the surface and the transition region were likely to be above this value. If a lower value of base hardness was chosen, results would not change significantly as the transition region for AISI 4140 was found to be generally small. If a higher value than 50 HRc were chosen the case depth reported could have been influenced by local material inconsistencies and the case depth may have been understated for some tests.

For all tests the measured hardness was between 56 and 66 HRc within the hardened region. Hardness at these values corresponds well with the expected hard-

ness for martensite of a 40% carbon steel which is approximately 60 HRc [74]. The presence of non-martensitic phases is not evident as lower hardness readings would be expected in the hardened layer. Although, it was expected that some fraction of retained austenite was present, it has not shown to decrease hardness. Retained austenite would be more evident with a higher carbon steel, and fractions greater than 50% would significantly reduce the hardness [75].

Overall, good agreement was found when the hardness depth was compared to the transition line from martensite to ferrite/pearlite. Figure 4.13 shows the hardened depth for a test run at 400 W laser power and 1000 mm/min scanning speed. The measured hardened layer from the image is approximately 224 μm whereas the average case depth found from the micro-indentation hardness measurements was 213 μm.

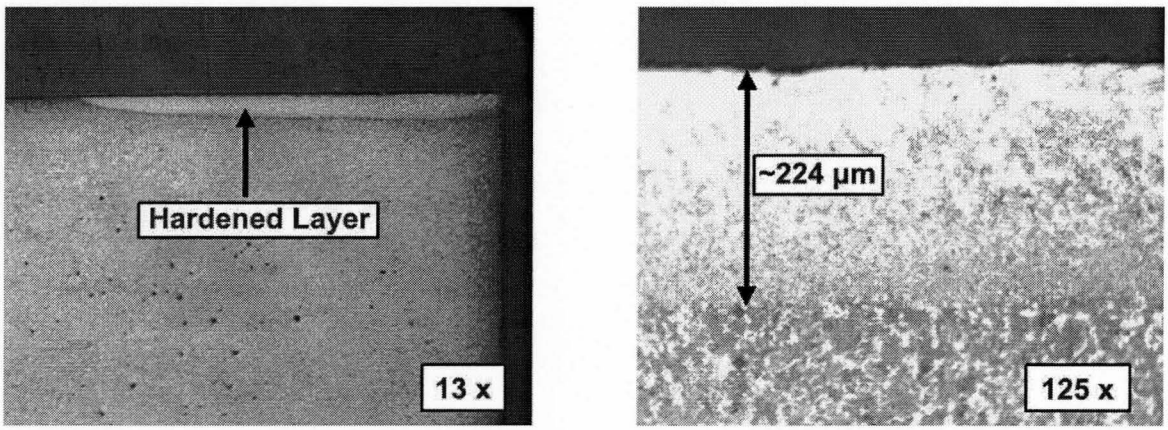

Figure 4.13: Hardened layer for 400 W laser power and 1000 mm/min scanning speed.

Modification of the case depth readings were made to account for surface alteration due to melting. Figure 4.14 shows four hardness profile measurements and Figure 4.15 shows the corresponding cross-section of samples taken at 2000 mm/min

scanning speed and a 1500 W laser power after one pass. Hardness readings displayed above the original surface are located in a layer of previously molten steel that has solidified above the original surface. Of most concern is that some molten material has been displaced and left valleys peaking below the original surface plane. For practical purposes the size of the valley defines the minimum amount of material that would need to be machined or ground away from the workpiece surface so that the finished surface is level.

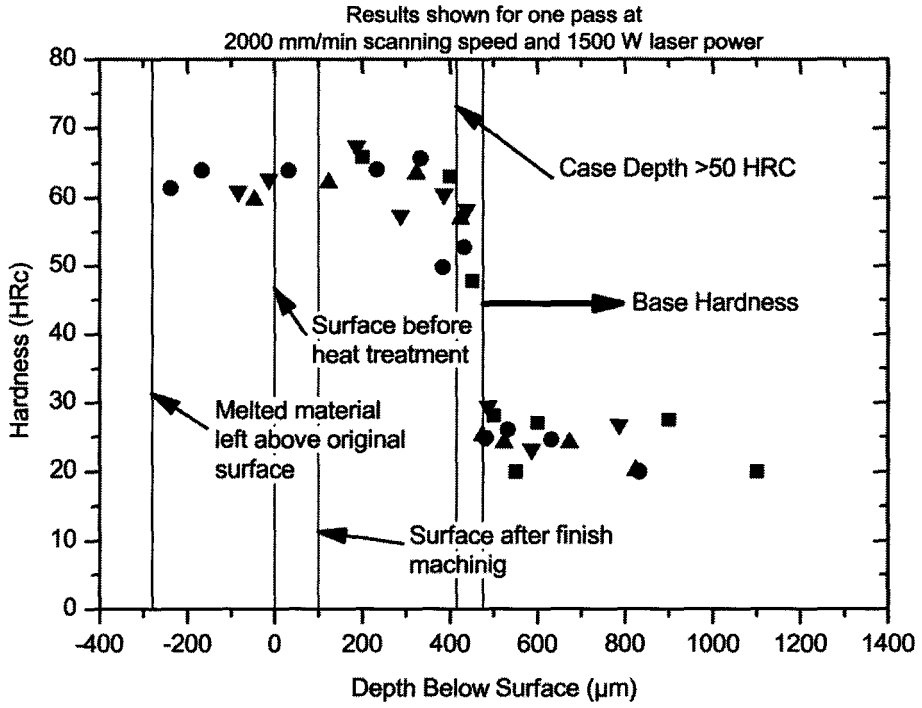

Figure 4.14: Hardness profile after one pass at 2000 mm/min with a 1500 W laser power showing hardened material layer before and after machining.

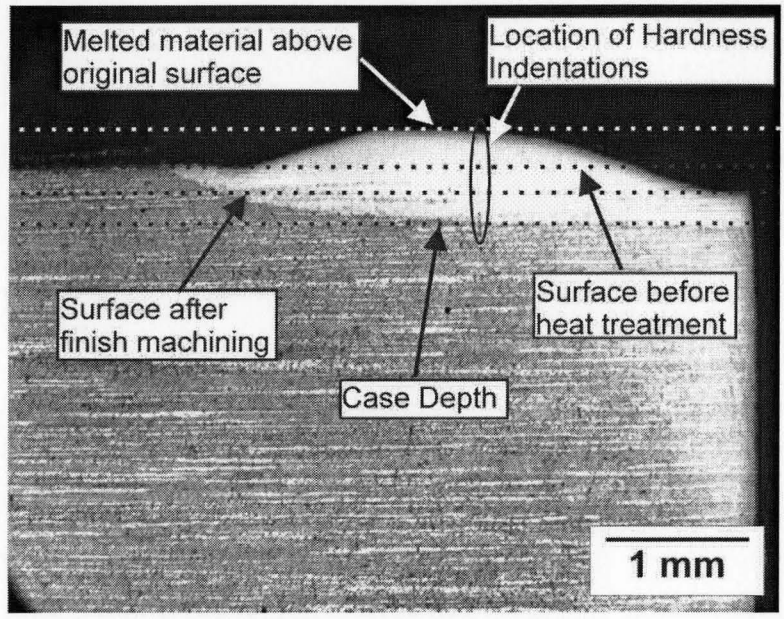

Figure 4.15: Cross-section after one pass at 2000 mm/min with a 1500 W laser power showing hardened material layer.

4.3.1 Slow Scanning Speed Tests

Results are shown for the slow series of tests in Figure 4.16 with the range bars indicating the standard deviation of the measurements obtained from four samples for each test condition. The results indicated that the predicted penetration depth was lower then actual for most tests. Since 910 °C is only a suggested value for full austenitization it is reasonable to believe that full austenitization could happen closer to the A_3 transformation temperature and result in higher case depths. This should be more evident with slower scanning speeds as more time is allowed for phase transformation. It is clear from Figure 4.16 that there is closer agreement between the predicted and measured case depths as the speed increases.

Minor material displacement from the edge of the workpiece defined the max-

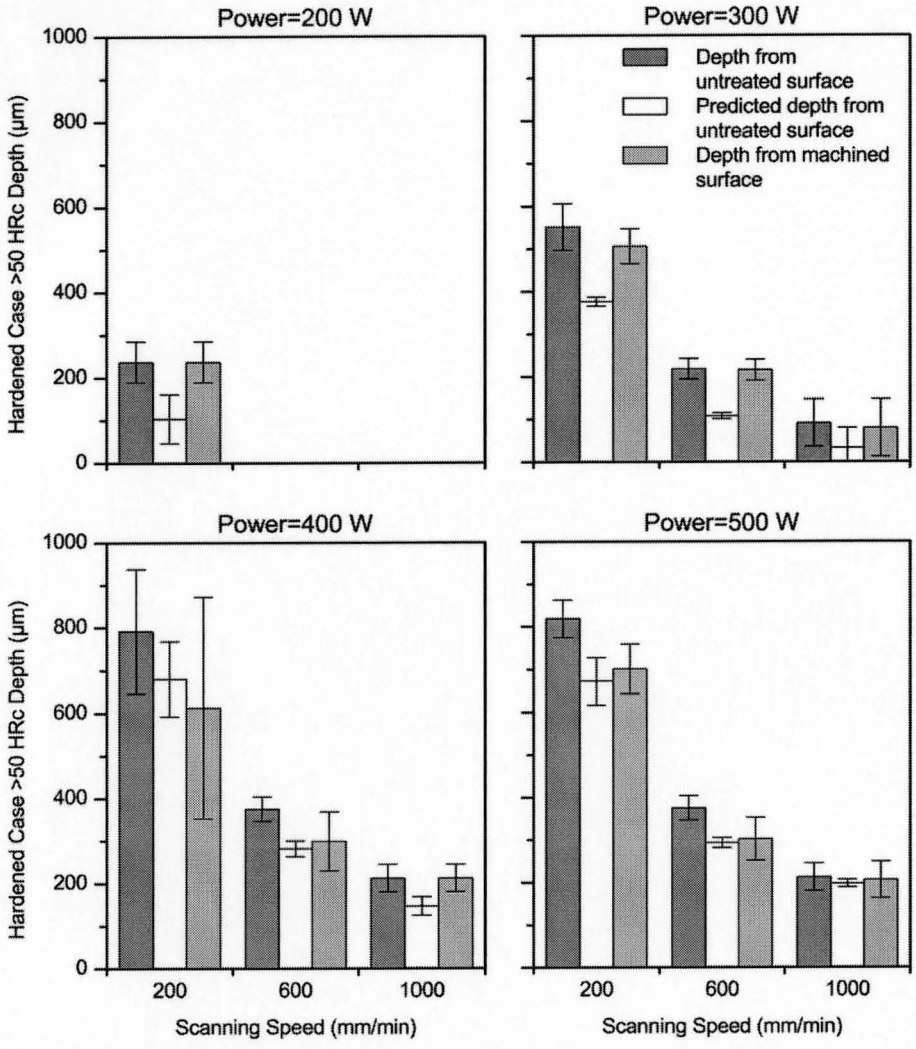

Figure 4.16: Predicted and measured hardness penetration depths for slow tests with low scanning speeds and low laser power.

imum final case depth after machining which is also shown in Figure 4.16. More material removal is required for lower scanning speeds and higher laser powers where melting was more prominent.

4.3.2 Fast Scanning Speed Tests (One and Two Passes)

Figure 4.17 displays the results for high scanning speed tests after both one and two laser passes. Higher case depths were possible after two laser passes as there was already heat built up in workpiece surface from the previous pass. Decreased rapid transformation temperature may also have existed as a result of continued austenite growth in the partially transformed transition region. Martensite transforms to austenite much faster than other phases because carbon is already well distributed within the iron matrix. This allows much faster austenite nucleation in regions of previously transformed material. This effect may be more evident in steels other than AISI 4140 that generally have much larger transition regions.

Although hardened cases were larger after two laser passes, there was a high degree of melting requiring a greater volume of material removal for the final machining stage. Therefore, the final case depths after finish machining for double pass tests were typically much lower than if only one pass was permitted. Only a small number of the tests performed predicted higher final case depths. These tests had lower laser power and higher scanning speeds and showed little or no melting. It may be reasonable to perform multiple laser passes if the melting temperature is not greatly exceeded. Manufacturing procedures that are restricted to staying near or below the melting temperature could obtain increased cases depths and thus benefit from multiple pass laser hardening.

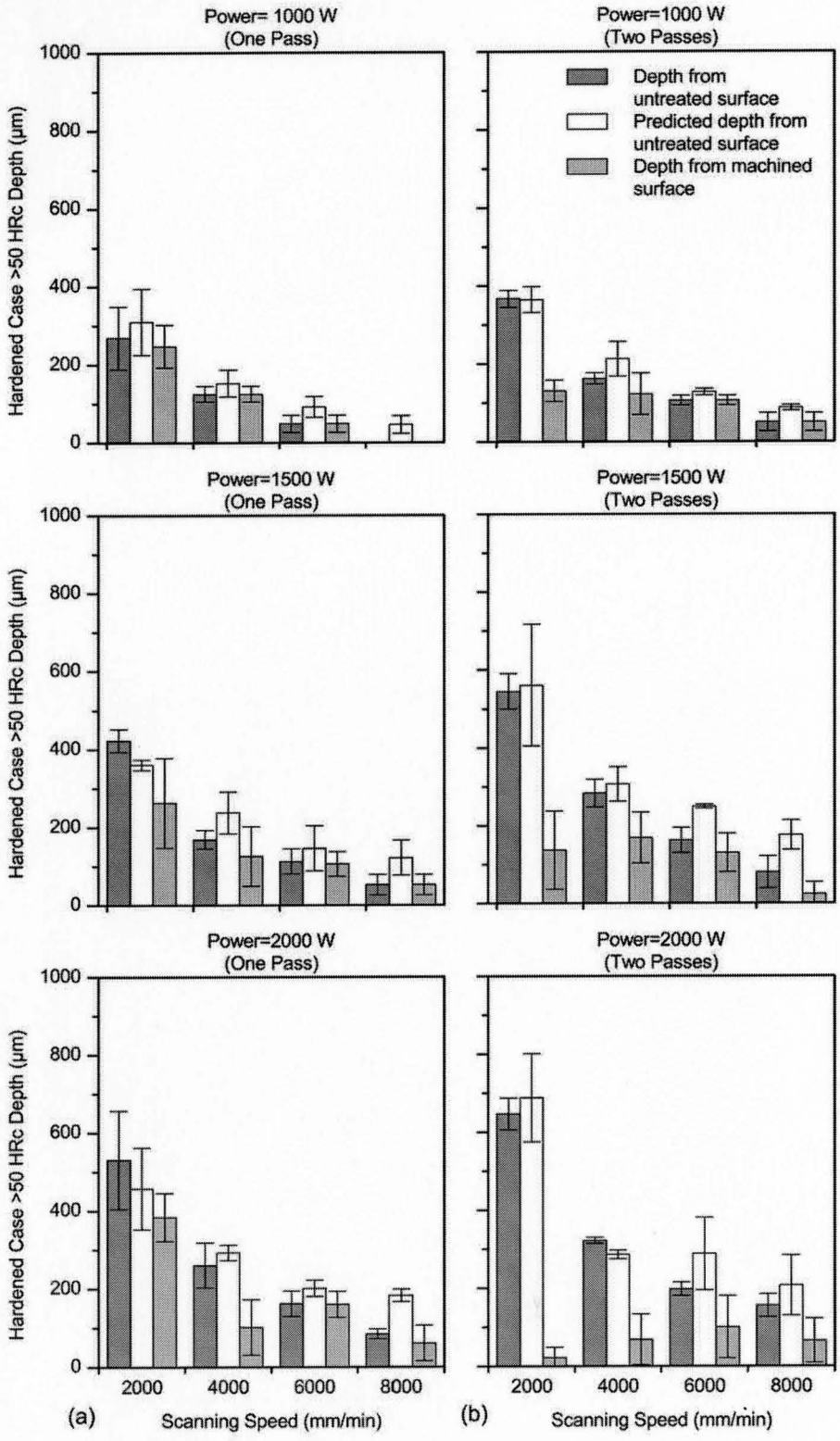

Figure 4.17: Predicted and measured hardness penetration depths after one and two laser passes for fast scanning speeds and high laser power.

If care was taken to maintain the surface temperature below the melting point and multiple passes were used the bulk material temperature would become a primary concern. If the bulk temperature was not maintained below a critical level there may not be a sufficient enough temperature gradient to induce rapid cooling. The resulting microstructure of the austenitized steel would be less martensitic consisting of bainite, ferrite and cementite phases, thus resulting in a softer microstructure.

The predicted measurements for high scanning speed tests shown in Figure 4.17 yield an over estimation of case depth. This becomes more apparent with increasing scanning speed. As with predictions for the slow scanning speed tests which showed underestimated predictions, time is critical for austenite formation. The faster scanning speeds reduce the heating cycle and the time that temperatures are above the A_1 and A_3 critical transformation temperatures. For full austenitization during rapid heating cycles it may be necessary to raise the temperature of the material to speed up the transformation rate. It is apparent that 910 °C cannot be used to assume full austenitization, as much higher temperatures are required when the scanning speed is high.

4.3.3 Austenite Equilibrium Temperature

Using the absorptivities and case depths found previously, the peak temperature at the case depth can be estimated using Jaeger's model. The case depth before finish machining was used to assume the deepest point at which the material was fully

austenitized. Figure 4.18 a illustrates the dependency of the equilibrium temperature on length of the heating cycle by comparing it with the scanning speed. Equilibrium temperatures nearly as low at the A_3 temperature (789 °C) were noticed for the slowest scanning speeds.

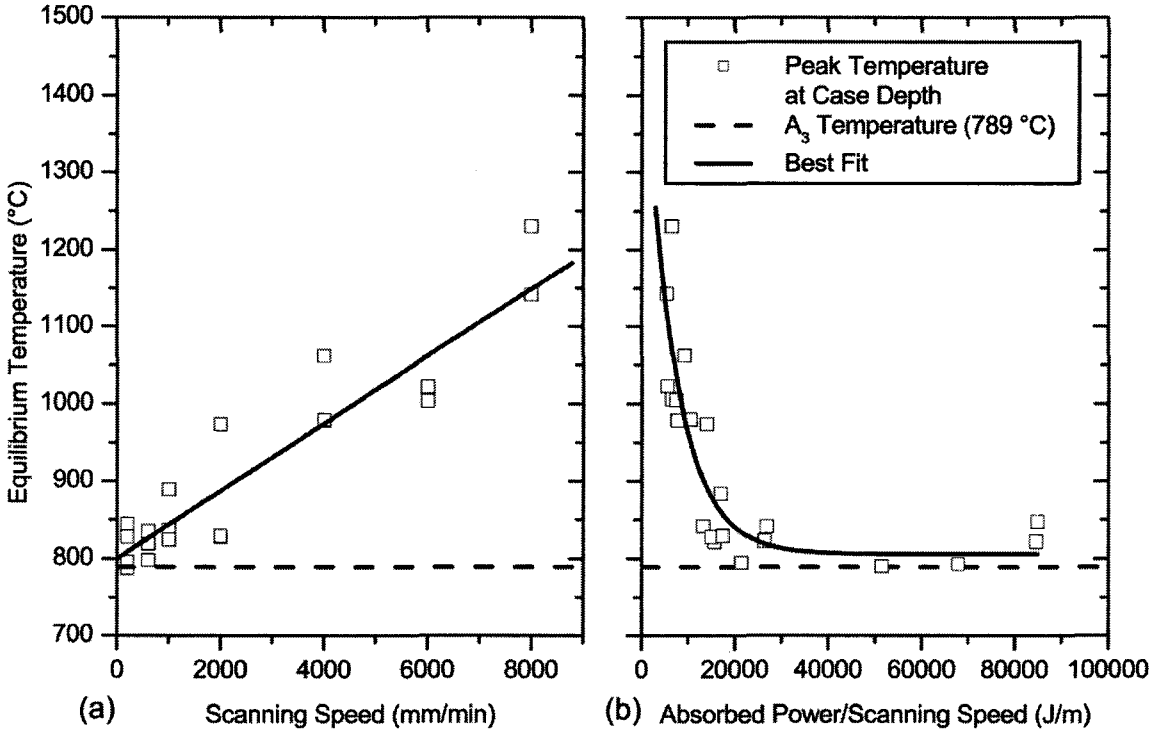

Figure 4.18: Adjusted transition temperature for full austenitization as a function of (a) scanning speed and (b) absorbed laser power/scanning speed from slow and fast tests.

To include any effects from the laser power, equilibrium temperature was shown in Figure 4.18b as a function of the ratio of absorbed power to the scanning speed (J/m). Here the transition exponentially decreases with increasing absorbed power over the scanning speed. Stability is reached above 20,000 J/m where the material can be assumed fully austenitized at temperatures above 850 °C, below 20,000 J/m

equilibrium temperatures as high as 1230 °C are shown. A more universal diagram could be developed if the effect of laser spot width were included. Spot width can have a great effect on the case depth and transition temperatures since it changes the laser work interaction time which is shown in equation 4.10.

$$\text{Laser Work Interaction Time (s)} = \text{Spot Width (m)} \,/\, \text{Scanning Speed (m/s)} \tag{4.10}$$

A larger spot width at the same total laser power will have a lower power density. This will allow more heat to be absorbed into the workpiece at lower temperatures, minimizing the need to exceed the melting temperature in order to minimize surface distortion. Equilibrium temperature will also be reduced as more time is available for austenite formation. However, if power density is too low there may not be enough energy to raise the temperature beyond the critical transformation temperature as heat is conducted into the bulk material too quickly.

As stated by Sandven [41], low power density and low scanning speed result in deep cases, but the cooling rate may be too low. If the cooling rate is too low it can lower the amount of formed martensite. For a low hardenability steel a high scanning speeds and a high beam density is necessary, but a shallower case will result. Spot width was not included in Figure 4.18b because it was maintained constant throughout this work but should be investigated in future work due to its important

influence on the process response and productivity.

4.3.4 Process Selection

As it was found that the transition temperature is a function of laser power and scanning speed it would be of practical importance to find a relationship for case depth. Figure 4.19 shows hardened depth as a function of laser power over scanning speed for both prior to machining and after. There is a strong enough dependence of case depth on laser power and scanning speed that this type of relationship could be used for initial process planning. The convenience of this type of graph is that it does not require any temperature measurement to calculate absorptivity, a task that can be the most difficult and time consuming. Using this diagram, process conditions can be chosen easily for a desired case depth. It is also suggested that laser width would be added to the comparison for greater detail.

The most negative aspect associated with the previous relationship is that experimental data is required for its formation. Figure 4.19 is expected to change with material type and surface finish. However, grouping the variables together minimize the number of experiments required to generate a new graph. A list of possible variables expected to affect the relationship shown in Figure 4.19 is as follows:

1. Workpiece material

2. Surface finish

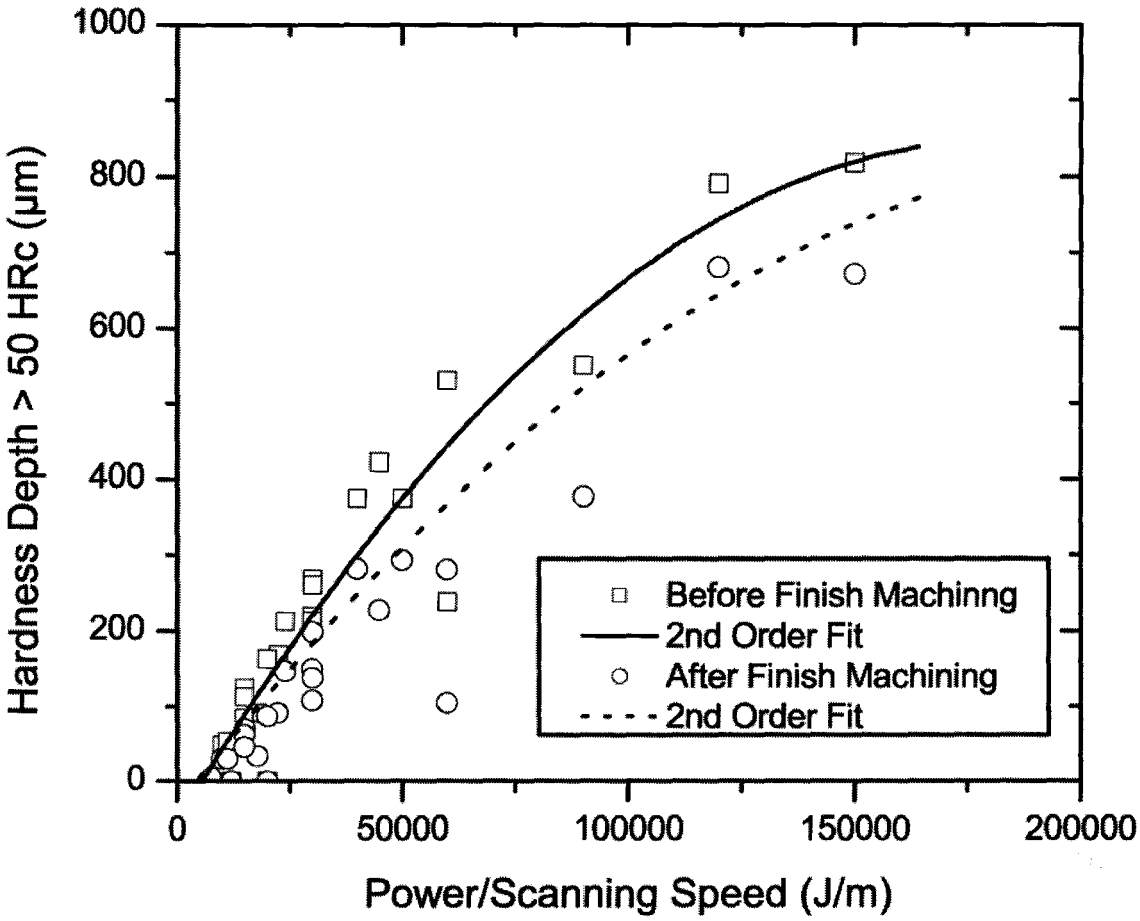

Figure 4.19: Case depth for slow and fast tests as a function of laser power and scanning speed.

3. Laser spot size

4. Workpiece geometry

4.4 In-Process Monitoring

Previous results indicate methods for choosing process parameters for a desired outcome. However, these results are not reliable enough if there are large geometrical differences in the workpiece from the experimental test pieces. It is also not possible

to use the previous results in order to estimate final treatment results and identify problems while the process is in progress. Meijer [57] identified that surface temperature could be used to predict the hardened case depth in-process. Combined with a closed-loop control algorithm this type of measurement could be very useful.

To show the relationship of case depth and surface temperature the hardened depth was plotted against peak surface temperature as shown in Figure 4.20. The results are shown for both slow and fast test series prior to any machining as in Figure 4.20a and after finish machining Figure 4.20b. Peak surface temperatures were obtained by calculations from the analytical model using the measured absorptivities.

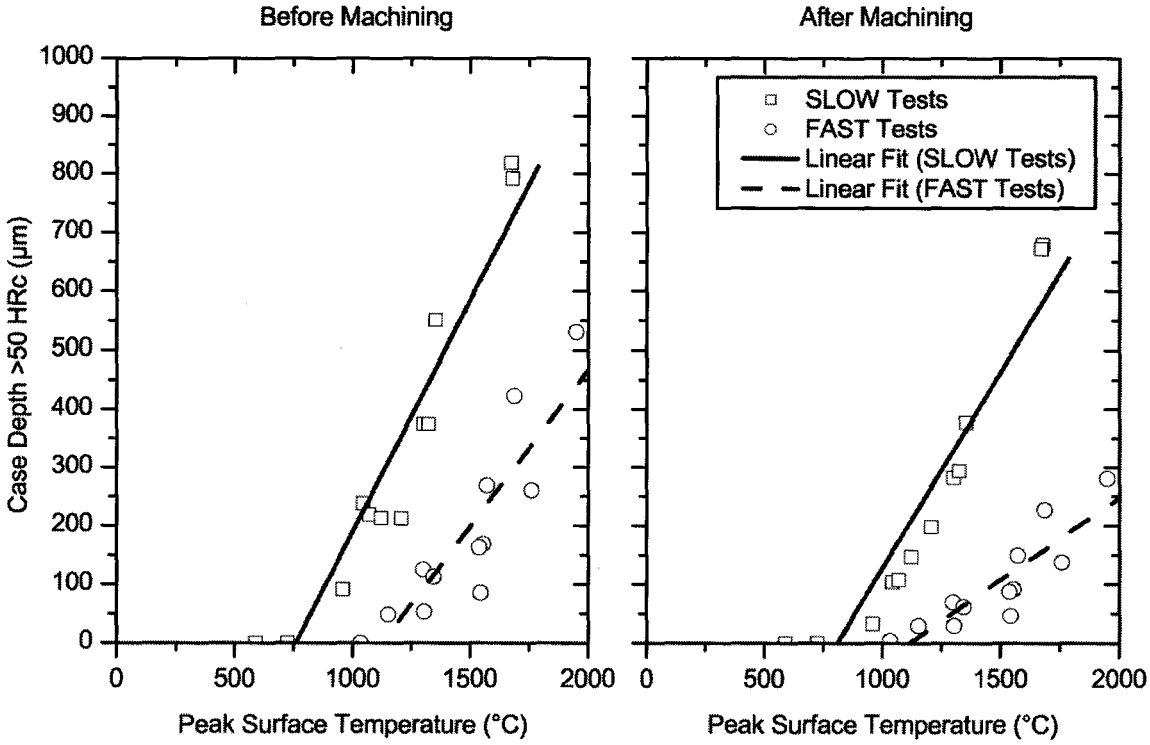

Figure 4.20: Hardened Depth > 50 HRc as a function of the peak surface temperature as obtained by analytical modeling.

Obvious linear trends arise in Figure 4.20 which is in agreement with Meijer's report. However, these trends are not useful in-process as they are based on calculations unrelated to the actual experiment. An infrared thermometer can be used to measure surface temperature without contact making it a convenient tool for this investigation. Not without problems, the infrared thermometer requires knowledge of the spectral radiant emissivity at the wavelengths sensed by the thermometer. Spectral radiant emissivity can change depending on the temperature, oxidation level, and melting. It is impractical to obtain this information for every case as this extra work defeats the purpose of in-process monitoring. Therefore, surface temperatures were measured by an infrared thermometer and were assumed to have an emissivity of 100%. This assumption underestimates the actual surface temperatures it is trying to measure. Although, this is not important if a relationship is found between case depth and the thermometer measurements and not with the calculated surface temperatures as shown previously. The measurements taken in process can then be compared with this relationship and corrective action can be taken if there is a problem.

For the slow test series the infrared thermometer was held stationary with the workpiece as the laser traversed the work surface. This resulted in a measurement that changed as the laser moved through the point that the thermometer was focused on. The peak reading of the temperature profile was chosen for comparison with the resulting case depth.

Fast test series experiments were measured with the thermometer fixed with respect to the laser as the workpiece rotated. The thermometer was focused on the laser spot to yield the highest possible measurement. The infrared thermometer was equipped with a spectral filter, limiting the sensitivity to radiation about 1.6 μm wavelength [76]. With this in consideration, reflected laser light was not expected to have an effect on the infrared measurements as the wavelengths of radiation emanated from the HPDL is much lower and within the range of 808 to 940 nm. A continuous measurement was recorded at the location of the laser spot. The average value of each data set was found and used for comparison with the case depth.

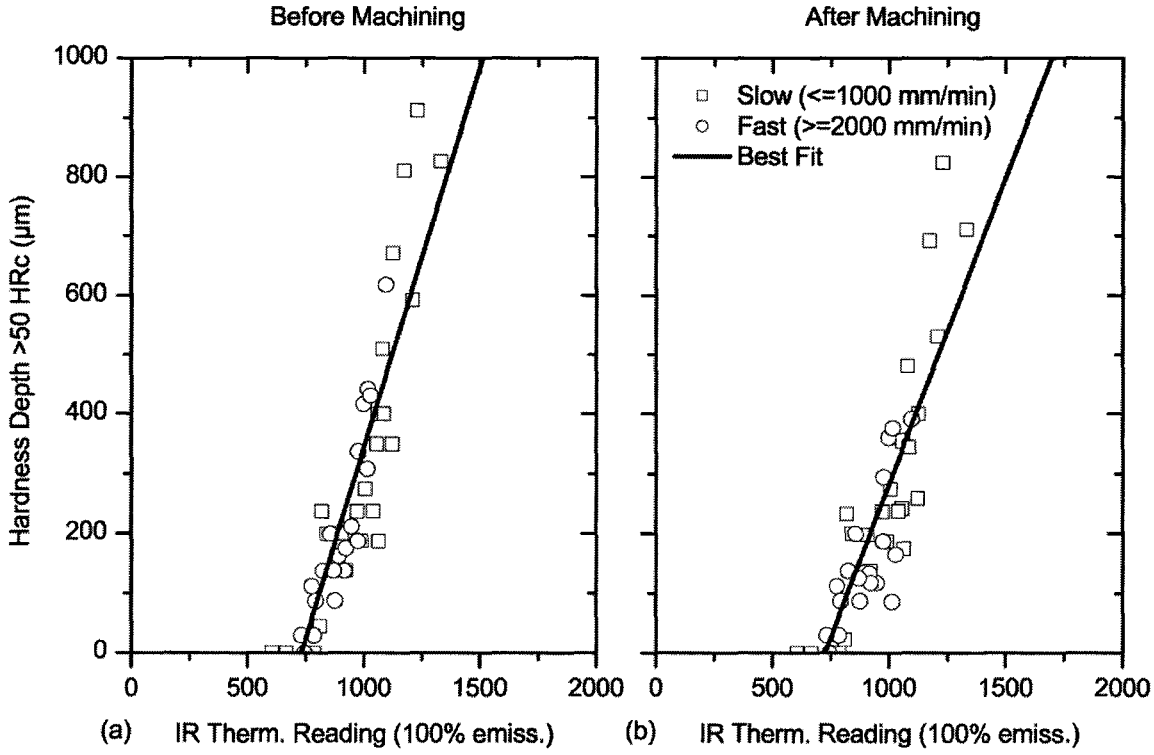

Figure 4.21: Hardened Depth > 50 HRc against the corresponding reading given by the infrared thermometer with 100% assumed emissivity, for fast and slow test series where (a) is before machining and (b) is after machining.

Figure 4.21 details the results for the case depth as a function of the infrared thermometer measurements. The linear trend shows good predictability. There is even close agreement between the slow and fast test series. From these results, infrared measurements appear to be independent of surface finish. As there are many problems related to describing the surface finish of a workpiece it can be very difficult or not feasible to use surface finish for prediction of absorptivity. It may be possible to use an infrared thermometer to aid in the calculation of absorptivity, but only after initial relationships are developed.

For double laser pass tests the infrared thermometer readings were averaged after the first pass and results are shown in Figure 4.22. Good predictability is indicated for the hardened case depth before any finish machining, but due to the large amounts of melting this method for prediction of case depth does not seem adequate. If temperatures were kept near or below the melting point then the validity of this procedure is restored. As melting is the primary concern when utilizing multiple passes, infrared measurements would be of benefit in order to control the degree of melting.

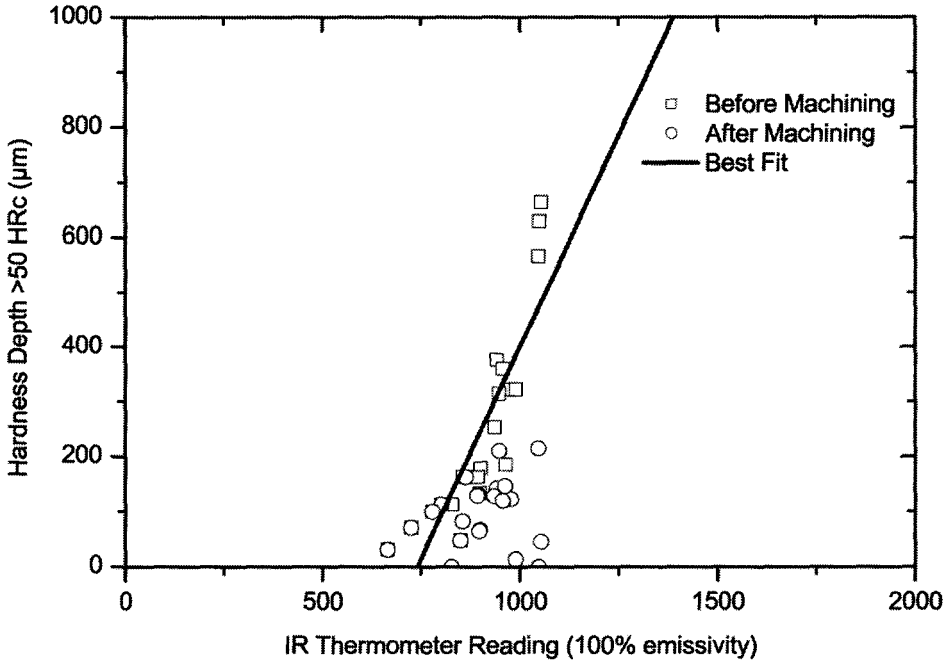

Figure 4.22: Hardened Depth > 50 HRc against the corresponding reading given by the infrared thermometer with 100% assumed emissivity, for the double test series, given prior and after machining.

CHAPTER 5
Conclusions and Future Work

5.1 Conclusions

Integrated machine tool laser hardening was investigated and found to have significant benefits over other surface hardening technologies. The increased flexibility and decreased lead times can greatly reduce costs. In this work, key problems associated with laser hardening were addressed. Three series of tests were performed including hardening at low laser scanning speeds on a linear workpiece and hardening with one and two laser passes at faster laser scanning speeds on a cylindrical workpiece.

Analytical and finite element models were developed and used to compare the experimental results with the calculated temperature profiles. Certain physical complexities beyond the original formulation of the analytical solution could not be added to the model. Thus, complexities such as temperature dependent thermal properties and surface heat losses were considered in the finite element model and the results were compared with those given for the analytical model.

To minimize error and computational time of the finite element model proper alignment of the laser beam with the surface elements was required. In addition, the element size had to be a multiple of the beam size so that there was a whole number of

elements within the laser spot. Increment size was also chosen so that this condition was maintained throughout the computational work.

It was found that the temperature profiles for the analytical model and the finite element model were in close agreement with the exception of the peak surface temperature, which was approximately 200 °C higher for the finite element model. The difference in peak surface temperature was further increased when temperature dependent thermal properties were included, but good agreement was still found for the remainder of the temperature profiles. Heat loss from the workpiece due to radiation was found to be negligible and could be excluded when modeling laser surface hardening. Furthermore, solving a transient finite element model was computationally more demanding than a quasi-steady analytical model. It was suggested that finite element modeling may be necessary if the accuracy of the peak surface temperature was important, otherwise an analytical model would be most often sufficient. For the purpose of this work high accuracy in the surface temperature was not required nor could this accuracy be verified through experiment.

A novel solution was used to measure the temperature profiles during the process. Lacquers that change appearance at a critical temperature were shown to yield reasonable and repeatable measurements for the tests. The analytical model was used to estimate the temperature profiles that best fit measurements of thermally indicative lacquers.

The fraction of absorbed laser power was found from the temperature measurements. High absorptivity (as much as 85%) was found for tests that were performed at low scanning speeds and low laser power. It was suggested that low surface temperature may more readily absorb laser energy than material at a higher temperature. Surface condition was also thought to play an important role on the absorptivity. More study is needed to identify physical reasons for the absorptivity of laser energy on a metallic surface and conditions that affect it.

The hardness profile was characterized for all tests. The largest case depths were found when the scanning speed was slow, but large amounts of melting were found for some tests, requiring finish machining. Melting was greatest for double pass tests and showed that multiple laser passes were only beneficial if the melting temperature at the workpiece surface was not greatly exceeded. Multiple laser passes can be used to increase hardened depth, if surface melting is undesirable.

Case depth predictions from the analytical model show that 910 °C cannot be used to assume full phase transformation to austenite. The case depth was under estimated for tests performed at slow scanning speeds and over predicted for faster scanning speeds. The equilibrium temperature for rapid heating was compared with the scanning speed and absorbed laser power. For high absorbed laser power and low scanning speeds the equilibrium temperature was close to that given by the iron-iron carbide phase diagram. For low absorbed laser power and high scanning speeds

equilibrium temperatures as high as 1230 °C were shown.

Case depth measurements before and projections after finish machining were plotted as a function of the laser power over the scanning speed. It is clear that this type of relationship can be used to help select process parameters. The relationship would be more useful if the spot width were included, as changing the spot width can have a positive effect on case depth.

Measurements from the infrared camera proved to have some ability to monitor the case depth. Infrared thermometers could be used to measure the progress of a hardening process on the fly. The results do not vary between the slow and fast tests sets and indicate that they may be independent of surface finish. This would allow thermometer measurements to be compared with the same relationships between tests having different surfaces.

5.2 Future Work

In order to choose initial process parameters the spot width should be added to the relationship for case depth as a function of laser power and scanning speed. An investigation should be made into the limits that material hardenability impose on the power density and laser interaction time.

Since it is a major factor on the workpiece absorptivity, the effect of surface finish should be investigated. Performing the process in a machine tool allows for a wide variety of surface finishes to be generated easily. If the effect of surface finish is better

understood, machining conditions could be chosen to maximize the effectiveness of laser hardening. This advantage should be developed and used to its full potential.

The development of a control algorithm for use with the infrared thermometer should be studied. The control algorithm could be used to maintain the desired case depth by adapting the laser power and scanning speed. It could be used to maximize scanning speed to increase productivity and reduce melting levels in order to maintain the depth of cut for finish machining. For multiple laser passes the control system could be used to maintain surface temperature as melting is of great concern.

Coatings could be studied as they can increase absorptivity. If coatings are chosen that contain desirable elements, these elements could interact with the workpiece surface upon heating with the laser. Laser alloying could increase carbon or nitrogen content, thus increasing the hardness potential of low alloy steels. Nitrogen could also be applied to the laser-work region as a gas. Diffusion of the nitrogen into the workpiece could be developed into a laser nitriding process.

An additional problem that can limit the practical implementation of laser hardening should be addressed. Back tempering at the edge of the hardened zone can occur due to adjacent laser passes. The tempered material is at a lower hardness and may be undesirable. On the other hand, this could be beneficial as this region may be used to retain lubricants when the hardened surface is between sliding contacts. Modeling may be useful to investigated the formation of the back tempered zone. Control and

limitation of this zone should be studied. Applications that may benefit from this phenomenon need also be investigated.

References

[1] H. Hügel, M. Wiedmaier, and T. Rudlaff. Laser processing integrated into machine tools - design, applications, economy. *Optical and Quantum Electronics*, Vol. 27:pp. 1149–1164, 1995.

[2] J.C. Ion. Laser transformation hardening. *Surface Engineering*, Vol. 18:pp. 14–31, 2002.

[3] Lin Li. Advances and characteristics of high-power diode laser materials processing. *Optics and Lasers in Engineering*, Vol. 34:pp. 231–253, 2000.

[4] P. Loosen et al. High-power diode lasers and their direct industrial applications. *Proceedings of SPIE - The International Society for Optical Engineering*, Vol. 2382:pp. 78–88, 1995.

[5] P. Koshy and P. Dumitrescu. A simple technique to characterize the role of work hardness in hard part machining. *Journal of Engineering Manufacture*, Vol. 217:pp. 1485–1489, 2003.

[6] J.O. Arnold and A. McWilliam. The thermal transformations of carbon steels. *The Journal of the Iron and Steel Institute*, Vol. 68:pp. 27–83, 1905.

[7] G.A. Roberts and R.F. Mehl. The mechanism and the rate of formation of

austenite from ferrite-cementite aggregates. *Transactions of the ASM*, Vol. 31:pp. 613–650, 1943.

[8] B. Karlsson and L.E. Larsson. Homogenization by two-phase diffusion. *Materials Science and Engineering*, Vol. 20:pp. 161–170, 1975.

[9] R.R. Judd and H.W. Paxton. Kinetics of austenite formation from a spheroidized ferrite-carbide aggregates. *Transactions of the Metallurgical Society of AIME*, Vol. 242:pp. 206–215, 1968.

[10] G.R. Speich, A. Szirmae, and M.J. Richards. Formation of austenite from ferrite and ferrite-carbide aggregates. *Transactions of the Metallurgical Society of AIME*, Vol. 245:pp. 1063–1073, 1969.

[11] M. Hillert, K. Nolisson, and L.E. Trndahl. Effect of alloying elements on the formation of austenite and dissolution of cementite. *Journal of the Iron and Steel Institute*, Vol. 209:pp. 49–66, 1971.

[12] A. Jacot, M. Rappaz, and R.C. Reed. Modelling of reaustenitization from the pearlite structure in steel. *Acta Materialia*, Vol. 46:pp. 3949–3962, 1998.

[13] W.J. Kaluba, R. Taillard, and J. Foct. The bainitic mechanism of austenite formation during rapid heating. *Acta Materialia*, Vol. 46(16):pp. 5917–5927, 1998.

[14] G. Molinder. A quantitive study of the formation of austenite and the solution of cementite at different austenitizing temperatures for a 1.27% carbon steel. *Acta Metallurgica et Materialia*, Vol. 4:pp. 565–571, 1955.

[15] R. Mancini and C. Budde. Reaustenitization in Fe-C steels revisited. *Acta Materialia*, Vol. 47:pp. 2907–2911, 1999.

[16] R. Mancini and C. Budde. Modelling reaustenitisation in Fe-C steels with concentration-dependent diffusivity of carbon. *Revista de Metalurgia (Madrid)*, Vol. 38:pp. 426–432, 2002.

[17] T. Akbay, R.C. Reed, and C. Atkinson. Modelling reaustenitization from ferrite/cementite mixtures in Fe-steels. *Acta Metallurgica et Materialia*, Vol. 42:pp. 1469–1480, 1994.

[18] C. Atkinson, T. Akbay, and R.C. Reed. Theory for reaustenitization from ferrite/cementite mixtures in Fe-C-X steels. *Acta Metallurgica et Materialia*, Vol. 43:pp. 2013–2031, 1995.

[19] B. D. Wakefield. Laser right on the beam for heat treating duty. *Iron Age*, Vol. 215:pp. 45–47, 1975.

[20] G.H. Harth III et al. Laser heat treating of steels. *Journal of Metals*, Vol. 28:pp. 5–11, 1976.

[21] C. Wick. Laser hardening. *Manufacturing Engineering and Management (Formerly Tool and Manufacturing Engineer)*, Vol. 76(6):pp. 35–37, 1976.

[22] Wineman J.A. Miller, J.E. Laser hardening at Saginaw-Steering-Gear. *Metal Progress*, Vol. 111:pp. 38–43, 1977.

[23] A. J. Hick. Rapid surface heat treatments - a review of laser and electron beam hardening. *Heat Treatment of Metals*, Vol. 10:pp. 3–11, 1983.

[24] E. Kennedy, G. Byrne, and D.N. Collins. A review of the use of high power diode lasers in surface hardening. *Journal of Materials Processing Technology*, Vol. 155-156:pp. 1855–1860, 2004.

[25] M. Haag and T. Rudlaff. Assessment of different high power diode lasers for material processing. *Proceedings of SPIE - The International Society for Optical Engineering*, Vol. 3097:pp. 583–591, 1997.

[26] F. Bachmann. High power diode laser technology and applications. *Proceedings of SPIE - The International Society for Optical Engineering*, Vol. 3888:pp. 394–403, 2000.

[27] F. Klocke, A. Demmer, and A. Zaboklicki. Investigation into the use of high power diode lasers for hardening and thermal conduction welding of metals.

Proceedings of SPIE - The International Society for Optical Engineering, Vol. 3097:pp. 592–599, 1997.

[28] B. Ehlers, H.J. Herfurth, and S. Heinemann. Hardening and welding with high power diode lasers. *Proceedings of SPIE - The International Society for Optical Engineering*, Vol. 3945:pp. 63–70, 2000.

[29] H. Pantsar and V. Kujanpää. Effect of oxide layer growth on diode laser beam transformation hardening of steels. *Surface and Coatings Technology*, Vol. 200:pp. 2627–2633, 2006.

[30] H. Pantsar and V. Kujanpää. Diode laser beam absorption in laser transformation hardening of low alloy steel. *Journal of Laser Applications*, Vol. 16:pp. 147–153, 2004.

[31] I.R. Pashby, S. Barnes, and B.G. Bryden. Surface hardening of steel using a high power diode laser. *Journal of Materials Processing Technology*, Vol. 139:pp. 585–588, 2003.

[32] S. Barnes, M.J. Nash, and Y.K. Kwok. Surface modification of powder metallurgy components with a direct diode laser. *Journal of Engineering Materials and Technology*, Vol. 125:pp. 372–377, 2003.

[33] J.C. Jaeger. Moving sources of heat and the temperature at sliding contacts. *Proceedings of the Royal Society of NSW*, Vol. 76:pp. 203–224, 1942.

[34] D. Rosenthal. Mathematical theory of heat distribution during welding and cutting. *Welding Research Supplement*, Vol.:pp. 220s–234s, 1941.

[35] D. Rosenthal. The theory of moving sources of heat and its applicatoin to metal treatments. *Transactions of the ASME*, Vol. 80:pp. 849–866, 1946.

[36] M.F. Ashby and K.E. Easterling. First report on diagrams for grain growth in welds. *Acta Metallurgica*, Vol. 30:pp. 1969–1978, 1982.

[37] J.C. Ion, K.E. Easterling, and M.F. Ashby. Second report on diagrams of microstructure and hardness for heat-affected zones in welds. *Acta Metallurgica*, Vol. 32:pp. 1949–1962, 1984.

[38] M.F. Ashby and K.E. Easterling. Transformation hardening of steel surfaces by laser beams-i: Hypo-eutectoid steels. *Acta Metallurgica*, Vol. 32(11):pp. 1935–1948, 1984.

[39] H.R. Shercliff and M.F. Ashby. Prediction of case depth in laser transformation hardening. *Metallurgical Transactions A (Physical Metallurgy and Materials Science)*, Vol. 22A:pp. 2459–2466, 1991.

[40] N.N. Rykalin, A.A. Uglov, and M.M. Nizametdinov. Calculation of the heating

of materials by laser radiation allowing for the temperature dependences of thermal properties. *Soviet Journal of Quantum Electronics (English translation of Kvantovaya Elektronika)*, Vol. 7:pp. 853–856, 1977.

[41] O.A. Sandven. Laser surface hardening. *ASM Metals Handbook, 10th Ed.*, Vol. 4:pp. 286–296, 1994.

[42] V.G. Gregson. Laser heat treament in laser materials processing. *Materials Processing Theory and Practices*, Vol. 3:pp. 206–219, 1983.

[43] H.E. Cline and T.R. Anthony. Heat treating and melting material with a scanning laser or electron beam. *Journal of Applied Physics*, Vol. 48:pp. 3895–3900, 1977.

[44] D.J. Sanders. Temperature distributions produced by scanning gaussian laser beams. *Applied Optics*, Vol. 23:pp. 30–35, 1984.

[45] I. Chen and S. Lee. Transient temperature profiles in solids heated with scanning laser. *Journal of Applied Physics*, Vol. 54:pp. 1062–1066, 1983.

[46] R. Festa, O. Manca, and V. Naso. Comparison between models of thermal fields in laser and electron beam surface processing. *International Journal of Heat and Mass Transfer*, Vol. 31:pp. 99–106, 1988.

[47] R. Festa, O. Manca, and V. Naso. Simplified thermal models in laser and electron

beam surface hardening. *International Journal of Heat and Mass Transfer*, Vol. 33:pp. 2511–2518, 1990.

[48] S. Kou and D.K. Sun. Heat flow during the laser transformation hardening of cylindrical bodies. *Metallurgical Transactions A (Physical Metallurgy and Materials Science)*, Vol. 14A:pp. 1859–1867, 1983.

[49] M. Lax. Temperature rise induced by a laser beam. *Journal of Applied Physics*, Vol. 48:pp. 3919–3924, 1977.

[50] H.S. Carslaw and J.C. Jaeger. *Conduction of Heat in Solids, 2nd Ed.* Oxford University Press, 1959.

[51] X. Tian and F.E. Kennedy. Maximum and average flash temperatures in sliding contacts. *Journal of Tribology*, Vol. 116:pp. 167–174, 1994.

[52] Z.B. Hou and R. Komanduri. General solutions for stationary/moving plane heat source problems in manufacturing and tribology. *International Journal of Heat and Mass Transfer*, Vol. 43:pp. 1679–1698, 2000.

[53] R. Komanduri and Z.B. Hou. Thermal analysis of the laser surface transformation hardening process. *International Journal of Heat and Mass Transfer*, Vol. 44:pp. 2845–2862, 2001.

[54] R. Komanduri and Z.B. Hou. Thermal analysis of laser surface transformation

hardening - optimization of process parameters. *International Journal of Machine Tools and Manufacture*, Vol. 44:pp. 991–1008, 2004.

[55] J. Mazumder. Laser heat treatment: The state of the art. *Journal of Metals*, Vol. 35:pp. 18–26, 1983.

[56] S. Kimura, Y. Nagano, N. Hoshina, and A. Kobayashi. Transformation hardening with CO_2 laser for the carbon tool steel. *Annals of the CIRP*, Vol. 28:pp. 109–112, 1979.

[57] J. Meijer and I. van Sprang. Optimization of laser beam transformation hardening by one single parameter. *Annals of the CIRP*, Vol. 40:pp. 183–186, 1991.

[58] J. Mazumder and W.M. Steen. Heat transfer model for CW laser material processing. *Journal of Applied Physics*, Vol. 51:pp. 941–947, 1980.

[59] W.M. Steen and C. Courtney. Surface heat treatment of En8 steel using a 2 kW continuous wave CO_2 laser. *Metals Technology*, Vol. 6:pp. 456–462, 1979.

[60] C. Maier, P. Schaaf, and U. Gonser. Calculation of the temperature profile for laser treatment of metallic samples. *Materials Science & Engineering A: Structural Materials: Properties, Microstructure and Processing*, Vol. A150:pp. 271–280, 1992.

[61] B.T. Chen, D.R. Huang, and S. Lee. Transient temperature profiles in a rectan-

gular thin film due to a scanning uniform strip heat source. *Journal of Physics D: Applied Physics*, Vol. 34:pp. 985–992, 2001.

[62] L.M. Galantucci and L. Tricario. Experimental and numerical study on the influence of not uniform beam energy distribution in laser steel hardening. *Annals of the CIRP*, Vol. 48:pp. 155–158, 1999.

[63] S.M. Rajadhyaksha and P. Michaleris. Optimization of thermal processes using an Eulerian formulation and application in laser surface hardening. *International Journal for Numerical Methods in Engineering*, Vol. 47:pp. 1807–1823, 2000.

[64] A. Yanez et al. Modelling of temperature evolution on metals during laser hardening process. *Applied Surface Science*, Vol. 186:pp. 611–616, 2002.

[65] W.B. Li, K.E. Easterling, and M.F. Ashby. Laser transformation of hardening of steel - ii: Hypereuctectoid steels. *Acta Metallurgica*, Vol. 34:pp. 1533–1543, 1986.

[66] J.C. Ion, H.R. Shercliff, and M.F. Ashby. Diagrams for laser materials processing. *Acta Metallurgica et Materialia*, Vol. 40:pp. 1539–1551, 1992.

[67] J.C. Ion, T.J.I. Moisio, M. Paju, and J. Johansson. Laser transformation hardening of low alloy hypoeutectoid steel. *Materials Science and Technology*, Vol. 8:pp. 799–803, 1992.

[68] J.C. Ion and L.M. Anisdahl. PC-based system for procedure development in laser transformation hardening. *Journal of Materials Processing Technology*, Vol. 65:pp. 261–267, 1997.

[69] O. De Pascale, C. Esposito, P. Boffi, and M. Lepore. Semi-emperirical method for predicting hardened case depths in laser heating heat treating. *Materials Chemistry and Physics*, Vol. 19(3):pp. 205–214, 1988.

[70] Automation Creations. Matweb, http://www.matweb.com, 2006.

[71] Omega Engineering. *The Temperature Handbook, 5th Ed.* Curtis Publishing, 2004.

[72] Love. *Radiative Heat Transfer.* Merril Publishing Company, Columbus OH, 1968.

[73] C.M. Klaren, J. Deere, and J. Nelson. Methods of measuring case depth. *ASM Metals Handbook, 10th Ed.*, Vol. 4:pp. 454–461, 1994.

[74] W.D. Callister. *Fundementals of Materials Science and Engineering.* John Wiley & Sons, Inc., New York, NY, 2001.

[75] G. Krauss. Microstructures and properties of carburized steels. *ASM Metals Handbook, 10th Ed.*, Vol. 4:pp. 363–375, 1994.

[76] Raytek. *Marathon Integrated High-Performance Infrared Thermometer - Operator's Manual.* Raytek Corporation, 2000.